Dylan Lucero

Are Marine Anoxic Events Recorded in the Late Devonian-Carboniferous Boundary in the South Portuguese Zone?

Masters Thesis

Advisors: Dr. Paulo Fernandes & Dr. Gilda Lopes

Universidade do Algarve

Faculdade de Ciências e Tecnologia

Marine and Coastal Systems Masters

2024

Abstract

The Devonian-Carboniferous Boundary (DCB) marks a mass extinction event that coincided with an oceanic anoxic event recognized worldwide. The stratigraphic sequence of the Pedra Ruiva sea cliff in the South Portuguese Zone near the Bordeira village dates back to the end of the Devonian and the start of the Carboniferous periods. To date, no study has been conducted to investigate the presence of oceanic anoxic events at this location during the DCB. Twenty rock samples were collected and analyzed from two outcrops from the Pedra Ruiva sea cliff. This thesis aims to identify and describe any anoxic event in this area. The results showed that during the DCB, the Southern Outcrop went through a decrease in the CIA values. An abundance of SiO_2, changes in the ratio of V/Cr, as well as an increase in the abundances of the heavy metals V, Cr, U, Al_2O_3, and the ratio of V/(V+Ni) were also observed. The Northern Outcrop does not show the same relation between the DCB and the calculated values and abundances. However, it does show a major spike in the CIA values after the DCB that corresponds to an increase in the V/C and V/(V+Ni) ratios, an abundance of SiO_2 and a decrease in Al_2O_3.The sedimentary facies of the two outcrops indicate that the proxies used to detect OAEs were deposited in non-ideal conditions for their preservation. Due to this the findings do not provide a definitive answer; however proxies indicate that a study in the more northern portions of the Tercenas Formation may yield better results.

Acknowledgements

I would like to thank my advisors Dr. Paulo Fernandes and Dr. Gilda Lopes for their assistance, insight, feedback, and encouragement during my writing process. With their patience and dedication I was able to write this thesis to the best of my ability.

Index

Contents

Abstract 1

Acknowledgements 1

Index 2

Contents 2
List of Figures 3
List of Tables 4
List of Graphs 4
Appendix 4
List of Abbreviations 4

1. Introduction 5

1.1. Motivation 5
1.2. Goals of the Study 6
1.3. Devonian-Carboniferous Boundary 6
1.4. Oceanic Anoxic Events 7
1.5. Paleogeography of the South Portuguese Zone 9
1.6. Geologic Background 11

2. Methods 12

2.1. Materials 12
2.2. Sampling Location & Collection 13
2.3. Sample Preparation 15
2.4. ActLabs Geochemical Analysis 16
2.5. Sediment Lithology Record & Interpretation 17

3. Results 17

3.1. Chemical Index of Alteration 17
3.2. Heavy Metals 18
3.2.a. Southern Outcrop 18
3.2.b. Northern Outcrop 20
3.3. Heavy Metal Ratios 23
3.3.a. Southern Outcrop 23

3.3.b. Northern Outcrop 24
3.4. Major Element Oxides 27
3.4.a. Southern Outcrop 27
3.5.b. Northern Outcrop 29
4. Discussion 32
4.1. Sedimentology 33
4.2. Chemical Index of Alteration 36
4.3. Major Element Oxides 37
4.4. Heavy Metals 37
4.4.a. Southern Outcrop 38
4.4.b. Northern Outcrop 39
4.5. Heavy Metal Ratios 40
4.5.a. Southern Outcrop 40
4.5.b. Northern Outcrop 41
5. Conclusion 42
References 44

List of Figures

- Figure 1 - Hypothesized landmasses during the Late Devonian period. (http://www.scotese.com) 10
- Figure 2 - Hypothesized landmasses during the Late Devonian period showing the tectonic plate activity during this time. (Golonka et al., 2019) 11
- Figure 3 - Geologic map of the South Portuguese Zone. (Oliveira, 1990; Oliveira et al., 2009) 12
- Figure 4 - Lithology of the Southern and Northern Outcrops with an image key naming the sedimentary structures seen in the outcrops. 14
- Figure 5 - Images of the Southern and Northern Outcrops of the Pedra Ruiva cliff sample site. 15
  - *5.a & 5.b - Northern Outcrop*
  - *5.c & 5.d - Whole sample site to show visual scale*
  - *5.e & 5.f - Southern Outcrop*
- Figure 6 - Images from laboratory preparations of samples. 16
  - *6.a - Agate mortar used crush samples into 10-micron sized sediments*
  - *6.b - Fresh rock samples after being cleaned of excess sediments*
  - *6.c - Plastic sample containers labeled after being filled with prepped sediments*

List of Tables

- Table 1 - CIA values of the samples collected from the Southern Outcrop. 18
- Table 2 - CIA values of the samples collected from the Northern Outcrop. 18
- Table 3 - Heavy Metal values observed in the Southern Outcrop. 19
- Table 4 - Heavy Metal values observed in the Northern Outcrop. 21
- Table 5 - Heavy Metal Ratios observed in the Southern Outcrop. 23
- Table 6 - Heavy Metal Ratios observed in the Northern Outcrop. 25
- Table 7 - Abundances of Major Elements observed in the Southern Outcrop. 28
- Table 8 - Abundances of Major Elements observed in the Northern Outcrop. 31

List of Graphs

- Graph 1 - Heavy Metals in samples collected from the Southern Outcrop compared against the CIA values and lithology. 20
- Graph 2 - Heavy Metals in samples collected from the Northern Outcrop compared against the CIA values and lithology. 22
- Graph 3 - Heavy Metal Ratios calculated in samples collected from the Southern Outcrop compared against the CIA values and lithology. 24
- Graph 4 - Heavy Metal Ratios calculated in samples collected from the Northern Outcrop compared against the CIA values and lithology. 26
- Graph 5 - Major Element abundances shown alongside the CIA values for the Southern Outcrop. 29
- Graph 6 - Major Element abundances shown alongside the CIA values for the Northern Outcrop. 32

Appendix 50

List of Abbreviations

- DCB - Devonian-Carboniferous Boundary
- OAE - Oceanic Anoxic Event
- ActLabs - Activation Laboratories
- CIA - Chemical Index of Alteration
- PR - Pedra Ruiva
- Al_2O_3 - Aluminium oxide
- SiO_2 - Silicon dioxide
- Fe_2O_3 - Iron (III) oxide/ferric oxide
- CaO - Calcium oxide
- Na_2O - Sodium oxide
- K_2O - Potassium oxide
- TiO_2 - Titanium dioxide
- MgO - Magnesium oxide/magnesia,
- P_2O_5 - Phosphorus pentoxide
- V - Vanadium
- Cr - Chromium
- Co - Cobalt
- Ni - Nickel
- U - Uranium
- Pb - Lead
- Th - Thorium

1. Introduction

1.1 Motivation

There are several reasons to investigate evidence of an Oceanic Anoxic Event (OAE) in the South Portuguese Zone's geologic record at the Devonian-Carboniferous Boundary (DCB). An exploratory geochemical study has yet to be conducted in this specific geologic boundary concerning this OAE. Consequently, there is a significant absence of geochemical data that help to elucidate if this OAE is present in the South Portuguese Zone geological record and what type of perturbations occurred in the global geochemical cycles, in this region. One of the ways that this study may help fill in data gaps is that the DCB is marked by a mass extinction event that is considered one of the Big Five mass extinction events. The results of this study could be used to help understand more about this mass extinction and what environmental changes were occurring in the South Portuguese Zone during the DCB.

There are also implications and motivations for this study, as anoxia in our oceans is a genuine problem today. Due to climate change and human activities, the rate and scale of OAEs have increased, negatively impacting marine life and humans. Knowing whether OAEs occurred in this area during the DCB may prompt more research into how OAEs impacted the South Portuguese Zone in this period.

Evidence of OAEs in our Earth's past also allows for more research to be done on the study of anoxic events today. This is because if scientists know when and where these events occurred, studies can look at what climatic and environmental factors lead up to these events and how local biological communities respond. This is important as we are facing an increase in anoxic events around the world at present due to climate change, coastal development, and increased nutrient pollution. By understanding how ecosystems and organisms in the past responded to anoxic conditions, predictions can be made on how today's ecosystems and organisms may respond and possibly adapt to these conditions. An exploratory thesis such as this opens the door for research on these topics to continue and benefit future generations.

1.2 Goals of the Study

This thesis is an exploratory study with two clear goals. The first is to uncover evidence of anoxic events in the rock record of the South Portuguese Zone at the Devonian-Carboniferous Boundary (DCB). The second goal is to use geochemical proxies to chronologically characterize any anoxic events that may be discovered. These goals will guide the research and contribute to the broader understanding of anoxic events in the South Portuguese Zone.

1.3 Devonian-Carboniferous Boundary

The Devonian-Carboniferous Boundary (DCB) can be represented in the sedimentary rocks deposited at the end of the Devonian Period and the start of the Carboniferous Period (Aretz & Corradini, 2021). Mass extinctions have marked boundaries between geologic periods, where many species go extinct relatively quickly (Begum, 2021). The drivers of many of these events are poorly understood; however, they almost always result in significant changes in Earth's climate. The End Devonian Mass Extinction Event marks the DCB, also known as the Hangenberg Crisis, and is considered the second-worst extinction event of the Devonian (Kaiser et al., 2006). One of the drivers for this extinction event is believed to have been caused by an increase in the diversity and biomass of new terrestrial plant species with complex root systems (Algeo & Scheckler, 1998). The development and spread of these plants led to the formation of mature soils, which until this time were either non-existent or in thin layers similar to desert soils (Algeo & Scheckler, 1998). With the development of these more complex plants, weathering regimes of terrestrial sediments also changed as these plants broke up more chemical compounds and minerals than previous plants could (Algeo & Scheckler, 1998). This change in the weathering regimes allowed these sediments and their nutrients and minerals to be more easily eroded by natural processes and deposited into waterways, which flowed into the ocean. In today's world, terrestrial nutrients and minerals are deposited into waterways, such as rivers, which flow into larger bodies of water, most notably the ocean. Another impact that the increase in plant biomass had during this time was climate change, as the Late Devonian has evidence of going through a cooling period that may have led to large-scale glaciation on the supercontinent of Gondwana (Chen et al., 2021; Isaacson et al., 2008; Streel, 2000). This would have been caused by plants' increased atmospheric carbon intake and retention via photosynthesis.

Another factor believed to have played a role in the End Devonian Mass Extinction event was the movement of continental plate tectonics. During this time, the continents moved closer, resulting in the closure and shrinking of oceans such as the Rheic (Rhenohercynian) Ocean (Domeier & Torsvik, 2014; Nance et al., 2012). The closures of oceans and seaways impact ocean currents and circulation as the pathways of these currents shrink and eventually disappear, thus stopping or redirecting these currents. These changes in ocean currents can cause global changes in climate as the world's oceans and their circulation play a significant role in climate regulation (Nasa, 2019). The cooling episode that led to a period of glaciation during this time may have also been, in part, caused by a change in ocean circulation due to the movement of the land masses present at the time (Joachimski & Buggisch, 2002; Brezinski et al., 2008). However, as mentioned earlier, it is widely accepted that an increase in plant biomass is the main cause of the cooling trend seen during the End Devonian. This cooling period could have resulted in glaciation on the southern supercontinent of Gondwana, which caused global sea levels to fall and rise periodically due to fluctuating climatic conditions (Brezinski et al., 2008; Isaacson et al., 2008; Streel, 2000). A change in sea level and temperature can also further impact ocean currents and circulation, such as slowing the flow or changing circulation patterns (Herrmann et al., 2004).

1.4 Oceanic Anoxic Events

Oceanic Anoxic Events (OAEs) are oceanic events where the oxygen (O_2) levels in an area of the oceans decrease to a point where all aerobic functions stop (Demaison & Moore, 1980). OAEs in the stratigraphic record are often associated with local and worldwide extinction events, as they more frequently occur during significant climatic and environmental changes (Aretz & Corradini, 2021). Anoxic conditions arise when there is a high rate of organic decomposition in an ocean area due to bacteria that use O_2 to decompose organic material (Millero, 2000). This is often a result of eutrophication, when excess nutrients enter marine systems from terrestrial systems and cause a boom of primary productivity, often in the form of a phytoplankton algae bloom (Pinckney et al., 2001). Once the bloom occurs, a combination of poor water circulation, often caused by the stratification of the water column, and the decay of dead phytoplankton causes the O_2 below the surface layer to decrease to hypoxic or anoxic

conditions (Water Resources, 2019). OAEs today are known as Dead Zones or Anoxic Zones by many people and occur in many different places around the world, with two well-known examples being the Baltic Sea and the Gulf of Mexico. These locations can show the negative impacts of anoxic conditions on local biological ecosystems and fisheries. The severity of the anoxic/hypoxic areas in the Gulf of Mexico and the Baltic Sea today is believed to be caused by anthropogenic activities such as agricultural practices and degradation of estuarine ecosystems. These activities allow excess nutrients to enter these ecosystems, similar to those discussed earlier that may have occurred during the DCB. Without O_2, most lives cannot survive as their bodies can no longer perform the aerobic functions required to sustain themselves.

During the Frasnian and Famennian stages of the Late Devonian, there were two notable events known as the Kellwesser, one of the Big Five mass extinction events, and the Hangenberg Crises, the extinction event that marked the DBC, which are both known to have evidence of large-scale anoxic events (Kaiser et al., 2006; Aretz, 2021). Fossil and stratigraphic records show that these events significantly impacted the marine communities during these times. With fossil records showing major faunal turnovers and the disappearance of reef communities, stratigraphic records show increased levels of organic-rich sediments, which can indicate anoxic events (Aretz, 2021). The Kellwasser Crisis, like the Hangenberg Crisis, occurred during the Late Devonian; however, this event took place about 15 million years before the Hangenberg (Sallan & Coates, 2010). The Hangenberg Crisis, while not considered as severe as the previous Kellwasser Crisis, is still considered to be a devastating biological crisis that resulted in the extinction of many organisms and the complete eradication of major groups such as placoderm fish (Sallan & Coates, 2010).

Scientists use a few indicators to look for evidence of OAEs in the geologic record. Some of these are physical indicators such as the color and size of sediments; for example, fine sediments such as shale that have black or dark green colors are often associated with OAEs in marine sediments (Singh et al., 2022). Geochemical indicators can also be tested to tell if evidence of OAEs is present at a specific stratigraphic level. For example, phosphorus (P) has often been linked to OAEs. This element can indicate increased eutrophication, leading to OAEs or decreased productivity in the water column. Different concentrations and levels of oxides in sediments can also be indicative of possible OAEs occurring at the time of deposition. MnO is an excellent example of an oxide that decreases in low-oxygen ecosystems, so low levels or an

absence of this oxide in sediments may indicate that the environment at the time was oxygen-depleted or anoxic (Ostrander et al., 2017; Rue et al., 1997). Oxides such as Al_2O_3 and SiO_2 can indicate the type of weathering happening when the sediments are deposited. Certain metals in marine sediments, such as uranium or vanadium, are also used to tell if there is evidence of an OAE in the stratigraphic layer being studied. Uranium (U), for example, has been shown to have limited enrichment in oxic environments, indicating that low concentrations of U in sediment show that the environment may have been well-oxygenated (Algeo & Maynard, 2004; Klinkhammer & Palmer, 1991).

Concerning the DCB, changes in weathering and increase in complex soils, as well as possible changes in ocean circulation, may have been major contributing factors for the OAEs known from this period (Aretz & Corradini, 2021; Algeo & Scheckler, 1998; Domeier & Torsvik, 2014). The presence of an OAE marked the DCB and the mass extinction that occurred during that time. Previous studies have found evidence for OAEs in similarly aged deposits in other locations worldwide (Aretz & Corradini, 2021; Caplan & Bustin, 1999). It is unknown whether an OAE occurred in the South Portuguese Zone during the DCB; however, other localities of similar age and types of rock deposits have evidence that they happened at this time in Earth's history so, they may be present in this locality as well (Aretz & Corradini, 2021).

1.5 Paleogeography of the South Portuguese Zone

The land area today known as Portugal was in a much different location during the Late Devonian. During this time, Portugal was believed to be located in the Southern Hemisphere, as indicated in Figure 1 by the red rectangle. During the DCB, the location that would one day become Portugal was a relatively shallow marine platform located north of the Gondwana supercontinent. The global climate during the Late Devonian is generally considered to have been warmer than today's climate. However, there was a cooling episode during the end of the Devonian period, which is believed to have been caused by an increase in terrestrial plant biomass (Chen et al., 2021; Joachimski et al., 2009; Isaacson et al., 2008). Based on the location indicated in Figure 1 and the knowledge about the global climate during the end of the Devonian period, it is likely that the climate of the area was warm with a cooling trend as the end of the Devonian period transitioned into the Carboniferous period.

The South Portuguese Zone was adjacent to the closing Rheic Ocean. The closing of the Rheic Ocean was due to the movements of tectonic plates through subduction and seafloor spreading. This is illustrated in Figure 2, which shows a map with the hypothesized areas of active subduction and seafloor spreading of the late Devonian paleogeography (Golonka et al., 2019) and indicates that during the end of the Devonian period, the Rheic was undergoing a loss in seafloor area due to subduction zones near the continental margins of Gondwana and Laurussia (Euramerica) (Golonka et al., 2019).

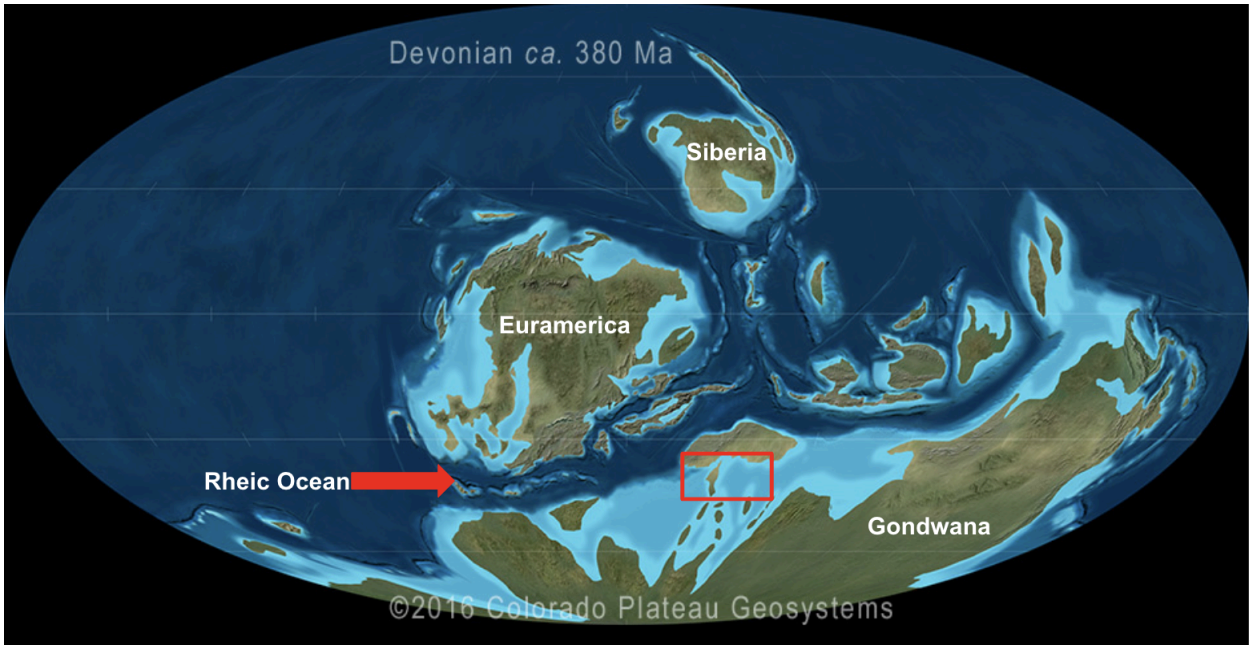

Figure 1: Hypothesized landmasses during the Late Devonian period. The red square on the map represents the area in which the South Portugal Zone was located. Source: http://www.scotese.com

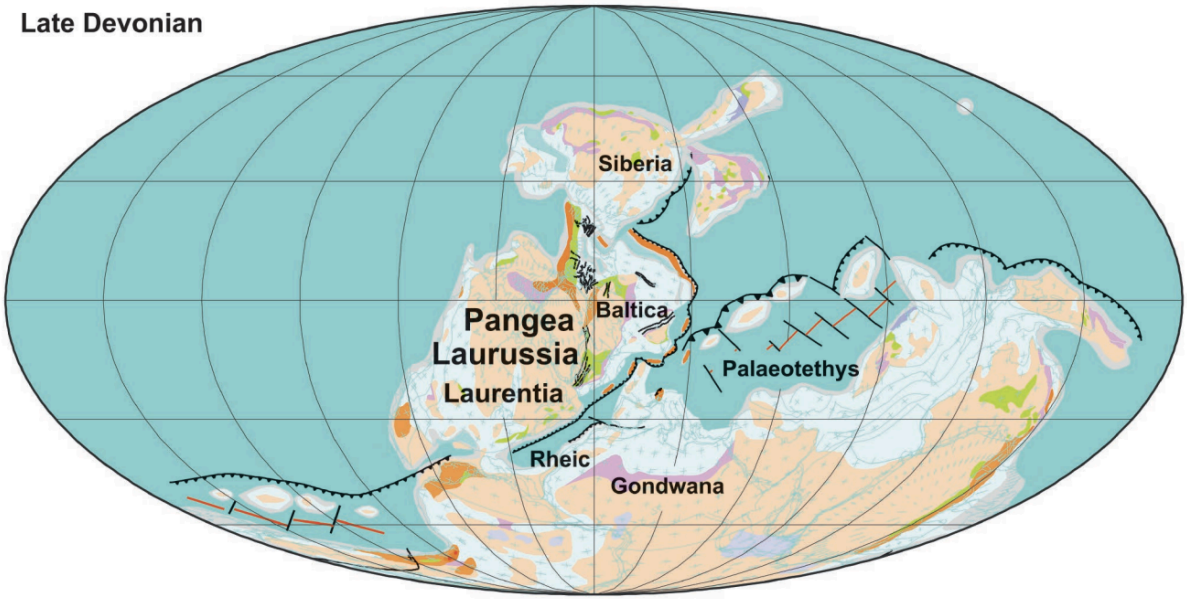

Figure 2: Hypothesized landmasses during the Late Devonian period showing the tectonic plate activity. Lines with triangles represent areas of active subduction. Red lines represent the seafloor spreading centers, and black lines represent transform faults. Source: (Golonka et al., 2019)

1.6 Geologic Background

The Tercenas and Bordalete formations of the South Portuguese Zone are dated to the Late Devonian-Early Carboniferous periods. The Tercenas Formation, dated to the Late Devonian, consists of heterolithic sandstone and shale facies, indicating sediment deposition in a tidal and nearshore environment. The Bordalete Formation, dated to the Early Carboniferous, is composed of dark shales, siltstones, and calcisiltstones, suggesting a less active and calmer depositional setting such as an offshore or outer shelf environment (Oliveira et al., 2009). Fossil fauna, including ammonoids and miospore biozones, were used to date these formations.

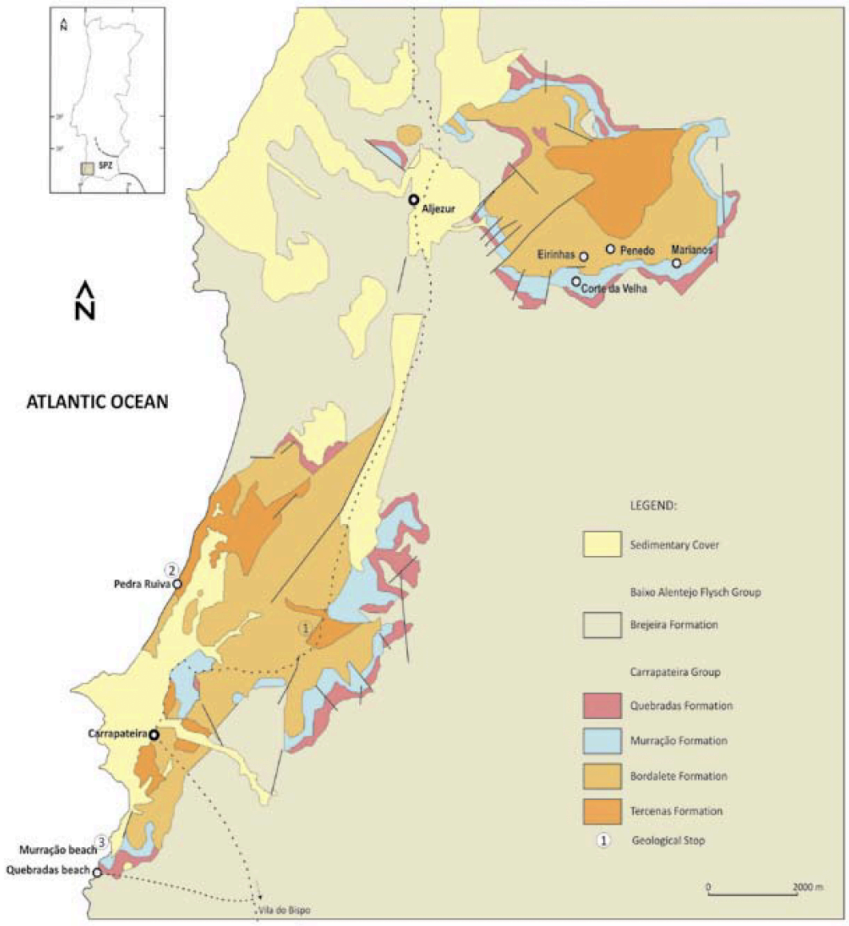

Figure 3: Geologic map of the South Portugal Zone showing the Pedra Ruiva sea cliff (labeled 2) as well as the Tercenas and Borbalete geologic formations. Source: (Oliveira, 1990; Oliveira et al., 2009).

2. Methods

2.1 Materials

Plastic Sample Bags	**Hammer and Chisel**
Hammer and Anvil	**Agate Mortar**
Scale	**Plastic Sample containers**
Sediment Spoon	**Sieve - 10 micron**

2.2 Sampling Location & Collection

Samples for this thesis were collected on the western coast of the Algarve in Portugal, near the Bordeira village. Twenty-one samples were collected, one being a control, and recorded by collection location. Within the sample site, rock samples were taken from the Northern and Southern outcrops of the Pedra Ruiva sea cliff. Only fresh rocks were collected directly from the cliff sides using a hammer and chisel. Extracted rock samples were then placed in bags labeled in the order in which they were collected (i.e., PR1, PR2, and so forth). The order in which the samples were collected was done in a way that samples started to be collected below the Devonian-Carboniferous Boundary and continued upwards past the boundary in numerical order, with the only exception being sample 20.

The composition of the sedimentary successions in both the Southern and Northern outcrops is shown in Figure 3. The sampled area of each outcrop is measured in meters, with the Southern Outcrop measuring just over 19 meters and the Northern Outcrop being just over 21.5 meters. Before the occurrence of the DCB in the Upper Devonian, both outcrops consisted mostly of claystone rocks with interbedded sandstone beds, also showing current ripple cross-lamination structures. The Southern Outcrop also has evidence of wave action in wave ripple cross-lamination structures; meanwhile, the Northern Outcrop shows evidence of minor bioturbation. After the DCB and into the Lower Carboniferous, the two outcrops start showing much more varied sedimentology between the two. The Southern Outcrop changes from mostly being composed of claystones to mostly sandstone and is very diverse in the sedimentary structures. Near the top of the Southern Outcrop, a small portion of siltstone is also present at 17 meters high. The most common sedimentary structures in the Southern Outcrop after the DCB are horizontal parallel lamination and planar cross-bedding. Herring-bone cross-bedding and swaley cross stratification make up the rest of the sedimentary structures found in the Southern Outcrop post-DCB. An interesting feature that is also present in the Southern Outcrop is the presence of five erosional boundary zones found from around 7.75 meters to 16.5 meters. The Northern Outcrop's sedimentology remains mostly unchanged from the Upper Devonian until about 12.5 meters, at which point the sedimentology changes to sandstone, which shows horizontal parallel lamination, as well as Herringbone cross bedding, planar cross-bedding, which ends around 17.5 meters. Towards the top of the Northern Outcrop, both become claystone with an incursion of sandstone just below 18 meters.

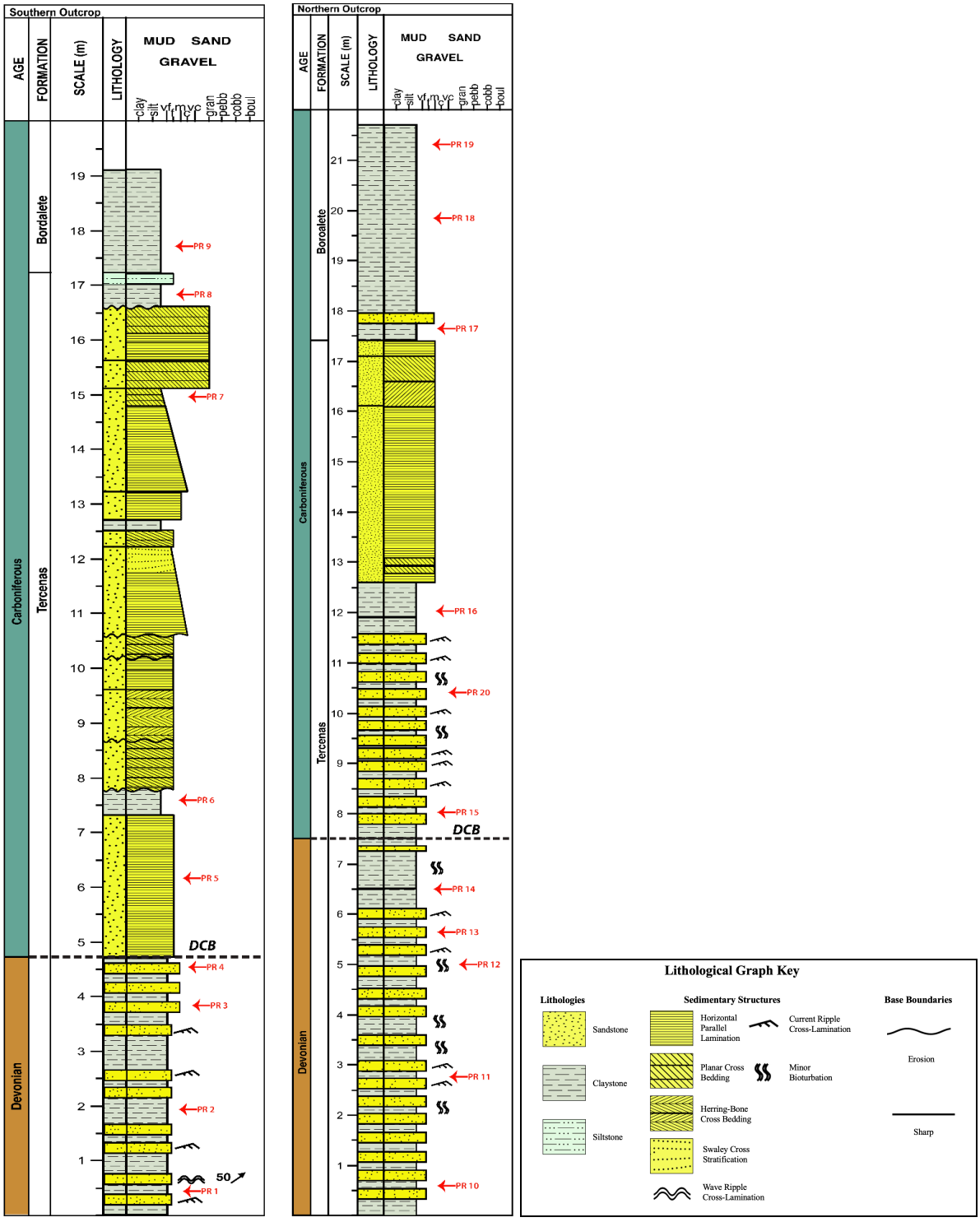

Figure 4: Lithology of the Southern and Northern Outcrops with an image key naming the sedimentary structures seen in the outcrops. Red arrows and references on the right indicate the samples studied.

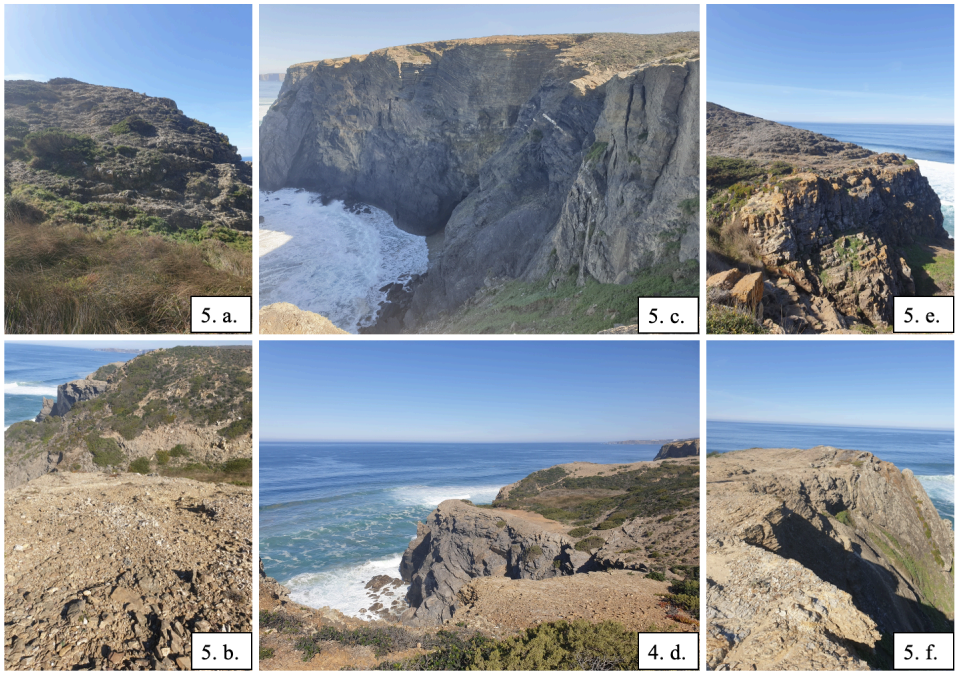

Figure 5: Images of the Southern and Northern Outcrops of the Pedra Ruiva cliff sample site. Images **5.a.** and **5.b** are of Northern Outcrop; images **5.e.** and **5.f.** are of the Southern Outcrop; images **5.c.** and **5.d.** are of the whole sample site for visual scale.

2.3 Sample Preparation

Samples were taken to the laboratory to be prepared for geochemical analysis performed by Activation Laboratories (ActLab) in Canada. Samples were rinsed in water to remove excess sediment dust and any other debris that may have been coating the samples. They were then crushed into smaller pieces using a hammer and anvil. Samples were then placed in a laboratory oven overnight to remove any excess moisture from the pores in the rock samples before crushing them further into finer dust. For this step, an agate mortar was used to crush each sample individually, after which the samples were sieved to remove any material larger than 10 microns. Samples were then placed in plastic vials, labeled, and weighed, with a weight goal of at least 19 grams; all equipment was cleaned between uses to eliminate cross-contamination between samples. Once all samples were prepared, they were shipped to ActLabs for analysis.

Figure 6: Images from laboratory preparations of samples: **6.a.** Image of agate mortar used to crush samples into 10 micron sized sediments **6.b.** Image of fresh rock samples after being cleaned of excess sediments **6.c.** Image of plastic sample containers labeled after filled with prepped sediments.

2.4 ActLabs Geochemical Analysis

The samples were analyzed for major and trace elements at Actlabs (Canada). The analytical procedures used were inductively coupled plasma-optical emission spectrometry (ICP-OES) for major elements analysis plus Ba, Sr, and Zr, and inductively coupled plasma-mass spectrometry (ICP-MS) for most trace elements. Alkaline dissolution was performed for all analyses, except for the determination of Cu, Ni, and Zn, for which acid digestion was carried out. The standards used were: NIST 694, DNC-1, BIR-1, FK-N, NIST 1633b, SY-3, W-2, NIST 696, JSD-3, CTA-AC-1, WMG-1, GXR-1, MICA-FE, GXR-2, LKSD-3, and MAG-1. The Appendix shows the analyses for three standard reference materials (BIR-1, W-2a, and DNC-1) and detailed limits for each element. The calculated reproducibility is bigger than 3% for major-elements contents (SiO_2, Al_2O_3, Fe_2O_3, MnO, MgO, CaO, Na_2O, K_2O and P_2O_5), ≈4% for

rare earth elements and ≈5% for high field strength elements. Additional information on analytical procedures is available at http://www.actlabs.com.

2.5 Sediment Lithology Record & Interpretation

To properly track the changes in the geochemistry of the DCB, a sediment log was created based on the sediment log made in a PhD thesis by Pereira (1997), using Sedlog and Adobe Illustrator once the results of ActLabs geochemical analysis had been delivered. DataGraph was then used to visually represent the data for the CIA values, major elements, heavy metals and heavy metal ratios. The graphs for CIA value, heavy metals, and heavy metal ratios were fitted and added to the sediment using Adobe Illustrator.

3. Results

All geochemical results provided by ActLabs can be found in the appendix at the end of this thesis.

3.1 Chemical Index of Alteration

The Chemical Index of Alteration (CIA) is a paleoclimate proxy that quantifies the extent of chemical weathering of sediment source areas using feldspar alterations (Nesbitt & Young, 1982). In order to determine the CIA, it is necessary to have the values for Al_2O_3, CaO, Na_2O, and K_2O. The CIA is calculated according to the equation:

$$CIA = \left(\frac{Al_2O_3}{Al_2O_3+CaO+Na_2O+K_2O}\right)\times 100$$

The CIA values in northern and southern outcrops show a general decreasing trend as the older Devonian strata pass to the younger Carboniferous. This decreasing trend then reverses as the sequences age. The south and northern outcrops have similar CIA values ranging between 70 and 80.5, with the lowest values mostly associated with the DCB.

Age	Sample Reference	CIA
Carboniferous	PR9	78.2
↓	PR8	77.0
↓	PR7	80.5
↓	PR6	77.7
DCB	PR5	77.0
DCB	PR4	77.0
↑	PR3	77.3
↑	PR2	79.5
Devonian	PR1	78.8

Age	Sample Reference	CIA
Carboniferous	PR19	79.2
↓	PR18	79.2
↓	PR17	78.6
↓	PR16	77.1
↓	PR20	78.7
DCB	PR15	77.0
DCB	PR14	77.4
↑	PR13	78.6
↑	PR12	79.0
↑	PR11	78.6
Devonian	PR10	79.7

Tables 1 & 2:
Table 1 shows the CIA values of the samples collected from the Southern Outcrop, Samples 1 to 9. **Table 2** shows the CIA values of the samples collected from the Northern Outcrop, Samples 10 to 20. The samples are organized in stratigraphic order.

3.2 Heavy Metals

3.2.a Southern Outcrop

According to the results of the analysis of heavy metal elements in the sediments of the DCB South Portuguese Zone, lead (Pb) and uranium (U) have the lowest values on average among all the heavy metals. Pb shows the lowest values, with most values falling below the detection limit of the analyzer instrument. There are only two values of 12 and 13 ppm, which are higher than the rest of the samples, while U has no values below 2.91 ppm or above 6.61 ppm. The Cobalt (Co) concentration in the samples ranges from 12 ppm to 33 ppm, with most values falling between 19 and 27 ppm. On the other hand, Nickel (Ni) concentration varies from 38 ppm to 71 ppm. Among the heavy metals, Vanadium (V) and Chromium (Cr) have the highest values. Most of the Cr values range from 100 ppm to 170 ppm, except for Sample 7, which has a

value of 70 ppm. The highest concentration is observed for Vanadium (V), with several samples having values above 200 ppm.

The results from the Southern Zone show a weak negative correlation between heavy metals V and Cr and CIA values, as displayed in Graph 1. This is observed in Samples 3 to 6, where CIA values decrease while V and Cr values increase. This change in the values also coincides with DCB. The other heavy metals shown in Graph 1 are unrelated to the CIA values. Most of the samples have a Pb value of zero, and U has remained at a relatively constant rate, with no significant changes in its values. The Co and Ni values do not correlate with the CIA values.

Focusing on the samples near the DCB and observing specific trends in these elements is possible. Looking at the U values, an upward trend leading up to the DCB during the Devonian can be seen. In contrast, after the sample which directly follows the DCB in the Carboniferous, a downward trend can be observed, as seen in both Graph 1 and Table 3. Together, this shows a spike in the sample values of U that coincide most closely with the DCB and inverse trends on either side of the DCB. Both the V and Cr show similar trends as U, which seem to increase during the Devonian, spiking around the DCB and going into a mostly downward trend during the Carboniferous as the samples get younger.

Age	Sample	Lead	Uranium	Cobalt	Nickel	Vanadium	Chromium
Carboniferous	PR9	0	2.97	12	38	161	110
↓	PR8	12	3.87	13	46	154	100
↓	PR7	0	2.91	25	43	97	70
↓	PR6	13	4.30	27	53	134	100
DCB	PR5	0	6.61	32	44	202	160
DCB	PR4	0	6.20	19	45	211	170
↑	PR3	0	4.38	21	43	182	130
↑	PR2	0	3.64	33	71	220	120
Devonian	PR1	0	4.47	19	42	219	140

Table 3: Heavy Metal values observed in the Southern Outcrop organized by oldest samples at the bottom and young samples at the top. Values are measured in ppm.

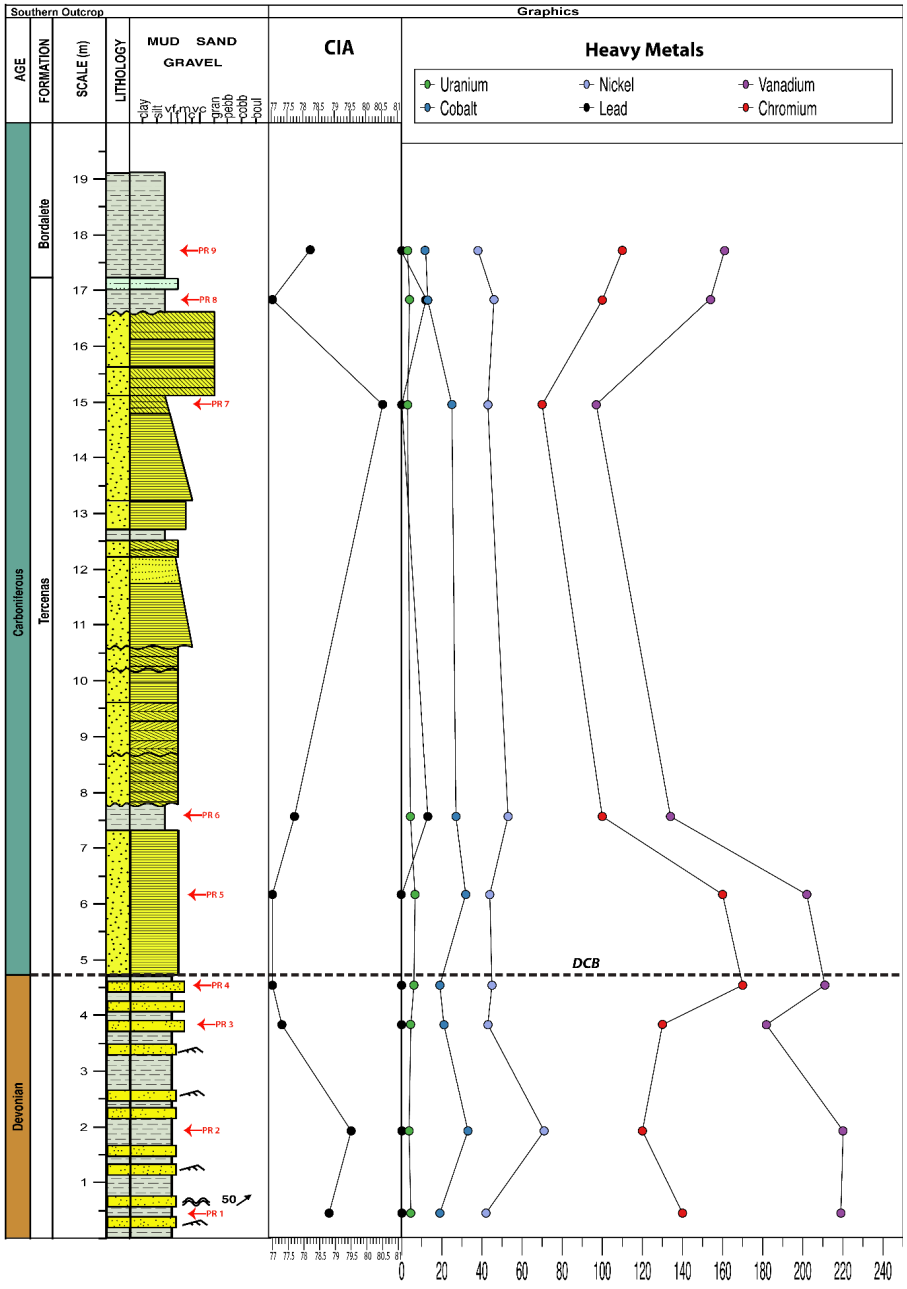

Graph 1: This a graphical representation of the Heavy Metals in samples collected from the Southern Outcrop compared against the CIA values and lithology.

3.2.b Northern Outcrop

The analysis of the samples from the northern outcrop yielded similar results from the southern zone, with a few exceptions. Pb and U had the lowest values recorded among the heavy metals, with Pb always having lower values than U. U values range between 2.50 ppm and 4.50 ppm. Most Co values in the northern outcrop are below 35 ppm, except for sample 13, which spikes at 69 ppm. Ni is noteworthy because while most values are at least 25 ppm, in sample

PR20, it drops to 8 ppm. The highest values of V and Cr for heavy metals in the northern zone are 176 ppm and 120 ppm, respectively.

Graph 2 for the Northern Zone shows a weaker positive correlation between the CIA and V than the Southern Zone. However, there is no correlation between the CIA and Cr in the Northern Zone. The heavy metals Pb and U exhibit similar behavior in the Southern Zone, with no observed correlations between CIA values and these two chemical elements. There is no correlation between the CIA values and Co and Ni. However, Ni and Co exhibit a positive correlation with each other as they experience similar drops and spikes.

Focusing on the DCB for the Northern Outcrop, the heavy metals Co and Ni, as mentioned in the previous paragraph, experience decreases and increases in values. Both V and Cr show a decrease in Sample 14, the oldest sample close to the DCB, and while both metals rise in value after the DCB, they do not appear to be correlated very strongly. After the DCB U has, on average, lower abundance than in the older Devonian samples. An increasing trend can also be observed in the older samples right before Sample 14; this pattern also appears for the Co and Ni values.

Age	Sample	Lead	Uranium	Cobalt	Nickel	Vanadium	Chromium
Carboniferous	PR19	9	2.65	2	25	166	110
↓	PR18	0	2.47	15	44	157	120
↓	PR17	5	2.54	2	27	176	120
↓	PR16	14	4.08	31	61	148	120
↓	PR20	0	2.91	1	8	165	120
DCB	PR15	7	3.43	29	58	122	100
DCB	PR14	0	3.08	15	42	105	100
↑	PR13	0	4.45	69	88	139	120
↑	PR12	0	4.16	26	54	139	120
↑	PR11	0	3.83	23	69	133	120
Devonian	PR10	7	2.62	26	86	171	110

Table 4: Table of the Heavy Metal values observed in the Northern Outcrop organized by oldest samples at the bottom and young samples at the top. Values are measured in ppm.

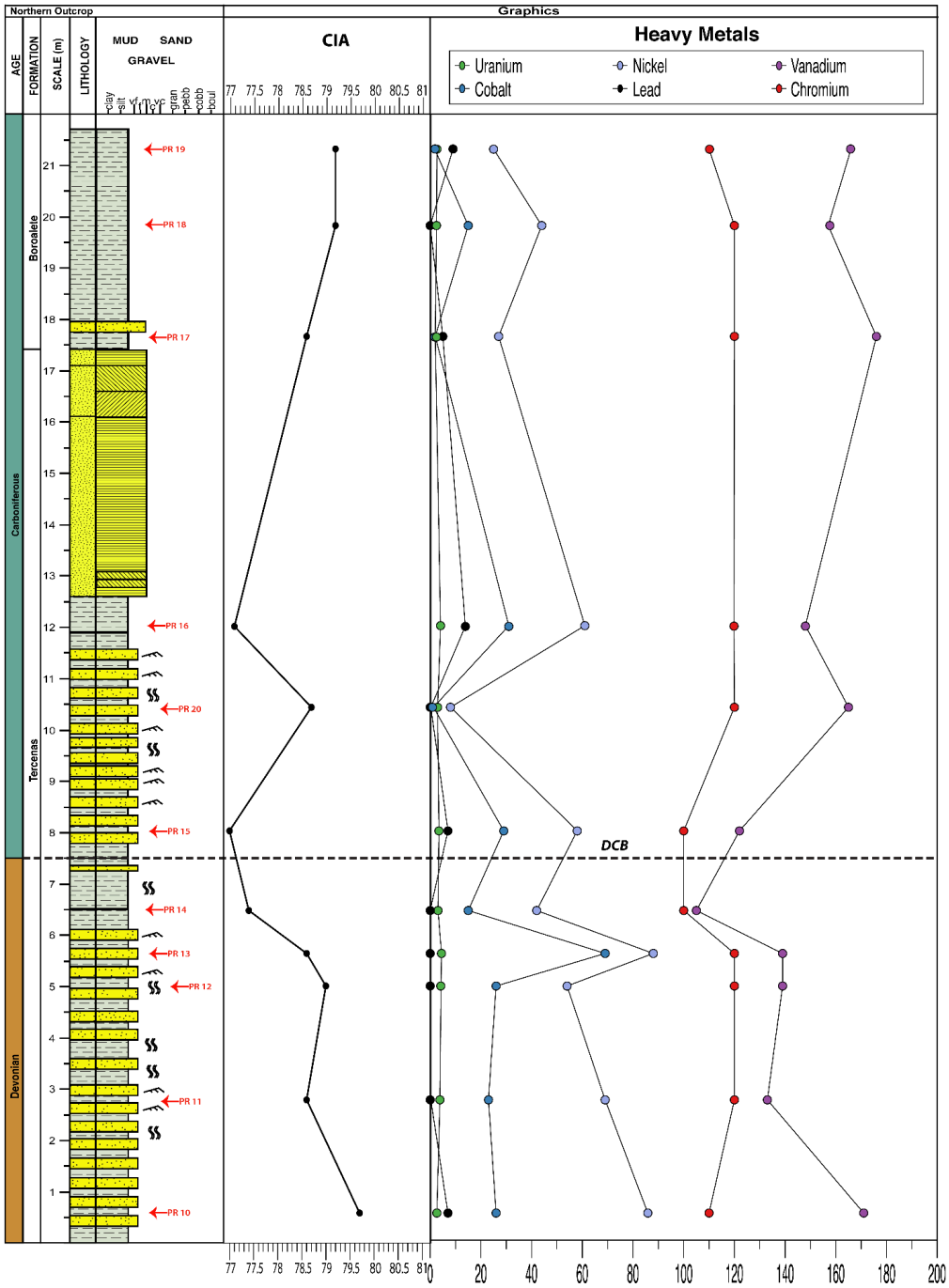

Graph 2: Graphical representation of the Heavy Metals in samples collected from the Southern Outcrop compared against the CIA values and lithology.

3.3 Heavy Metal Ratios

3.3.a Southern Outcrop

The U/Th ratio for all samples is between 0.20 and 0.22, except PR8, which is at 0.26. Vanadium and chromium (V/Cr) ratios range from 1 to 2, with the highest value at 1.58. Most values for V/(V+Ni) typically fall within the 0.80 range, except Sample PR7, which has a value of 0.69.

The Southern Heavy Metal Ratios graph shows that most value changes for this outcrop occur near the DCB. The values for U/Th remain relatively stable and do not undergo significant changes, except for Sample 4, the sample closest to the DCB. The V/(V+Ni) correlates negatively to the CIA values in the Southern Outcrop. Near the DCB, the V/(V+Ni) gradually increases from just before the DCB to the start of the Carboniferous. The V/Cr ratio values exhibit the most significant changes in this outcrop, particularly around the DCB. In the samples collected around the DCB, there is a continuous drop in the values of V/Cr from Sample 2 to Sample 3, with a decrease of 0.38. The ratio values increase after the DCB but reach different levels than samples 1 and 2.

Age	Sample	U/Th	V/Cr	V/(V+Ni)
Carboniferous	PR9	0.20	1.31	0.81
↓	PR8	0.26	1.40	0.77
↓	PR7	0.20	1.33	0.69
↓	PR6	0.22	1.15	0.72
DCB	PR5	0.22	1.10	0.82
DCB	PR4	0.22	1.10	0.82
↑	PR3	0.20	1.17	0.81
↑	PR2	0.20	1.55	0.76
Devonian	PR1	0.20	1.58	0.84

Table 5: Table of the Heavy Metal Ratios observed in the Southern Outcrop organized by oldest samples at the bottom and young samples at the top.

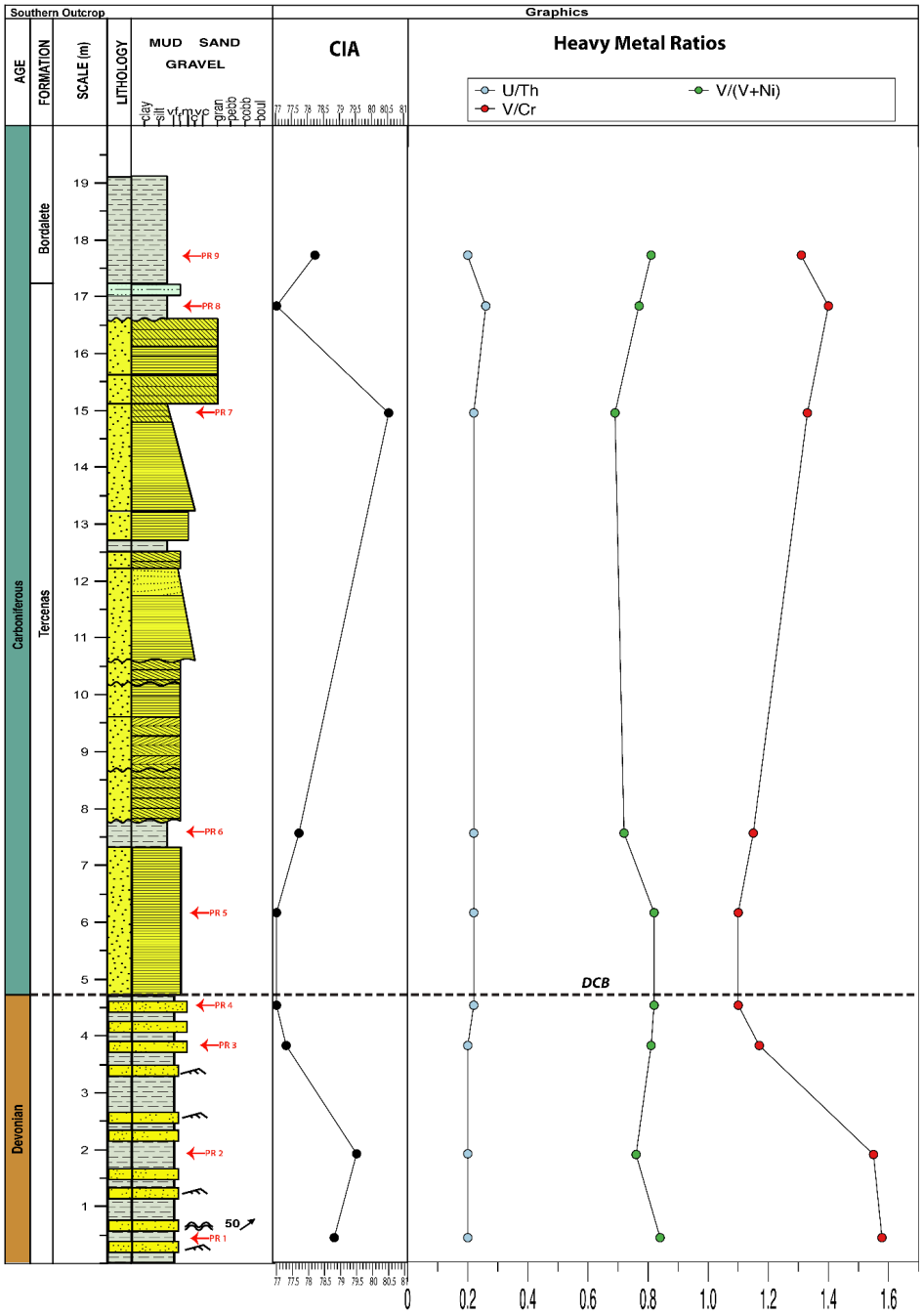

Graph 3: This a graphical representation of the Heavy Metal Ratios calculated in samples collected from the Southern Outcrop compared against the CIA values and lithology.

3.3.b Northern Outcrop

U/Th values are lower in the Northern outcrop (0.16-0.19) than in the Southern outcrop. The V/Cr values of the northern outcrop indicate a gradual increase as the samples get younger. Values below 1.10 are observed in all samples except for the PR10 sample, which has values

above 1.10. The northern outcrop's V/(V+Ni) ratio ranges from 0.61 to 0.95, with higher values concentrated in the younger Carboniferous samples.

The ratio values in the Northern Outcrop graph exhibit significantly more variation than those in the Southern Outcrop graph. Examining the U/Th values, it is evident that while there is a slight variation, the values remain relatively consistent throughout the Northern Outcrop. Throughout this outcrop, the V/(V+Ni) and V/Cr ratios exhibit significant variations in their values. V/(V+Ni) remains relatively stable until after the DCB, when it spikes from 0.68 (Sample 15) to 0.95 (Sample 20), and then drops to 0.71 (Sample 16). Although this spike appears location-based, it coincides with the CIA and V/Cr values spikes. The remaining samples exhibit a similar pattern concerning CIA, V/(V+Ni), and V/Cr. However, the V/Cr spike starts earlier than the CIA, and V/(V+Ni) begins before the DCB.

Age	Sample	U/Th	V/Cr	V/(V+Ni)
Carboniferous	PR19	0.16	1.38	0.87
↓	PR18	0.16	1.32	0.78
↓	PR17	0.17	1.45	0.87
↓	PR16	0.18	1.17	0.71
↓	PR20	0.17	1.42	0.95
DCB	PR15	0.19	1.18	0.68
DCB	PR14	0.22	1.04	0.71
↑	PR13	0.21	1.09	0.61
↑	PR12	0.21	1.07	0.72
↑	PR11	0.22	1.03	0.66
Devonian	PR10	0.19	1.34	0.67

Table 6: Table of the Heavy Metal Ratios observed in the Northern Outcrop organized by oldest samples at the bottom and young samples at the top.

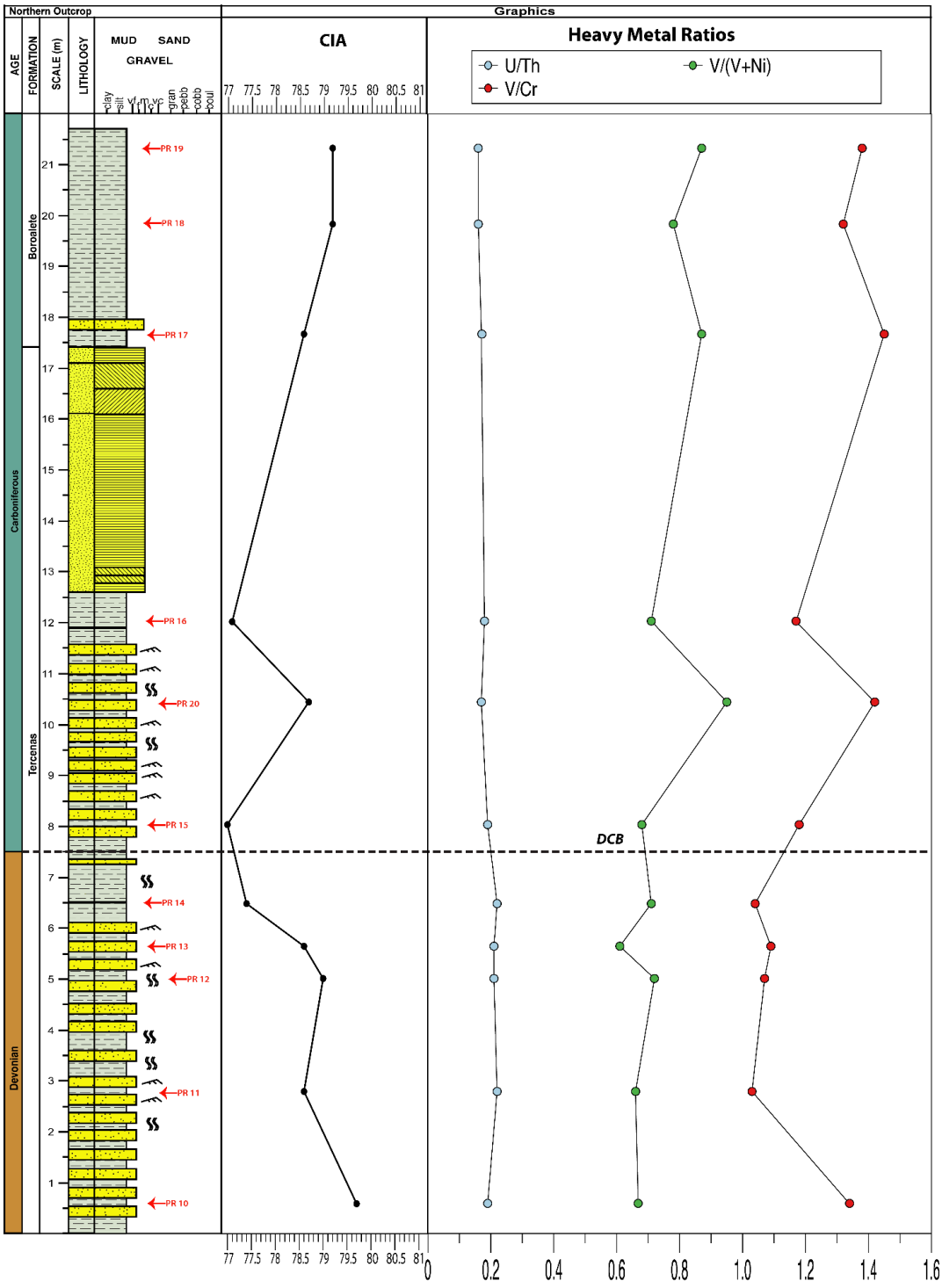

Graph 4: Graphical representation of the Heavy Metal Ratios calculated in samples collected from the Southern Outcrop compared against the CIA values and lithology.

3.4 Major Element Oxides

For the analysis of the major element oxides, the values for each were normalized to see the percentage abundance of these major elements in the Southern and Northern outcrops.

3.4.a Southern Outcrop

Graph 5 and Table 7 show that SiO_2 (silicon dioxide) has the highest abundance of the major elements; SiO_2 abundance ranges from 47.61% in PR 4 to 68.25% seen in PR 8. Al_2O_3 (aluminum oxide) is the second most abundant major element, with an abundance ranging from 18.77% in PR 8 and 34.78% in PR 8. Graph 5 shows a clear inverse correlation between SiO_2 and Al_2O_3, with this correlation being seen in the inverse curves in Graph 5 and the percentages from the table mentioned before. Fe_2O_3 (iron (III) oxide/ferric oxide) and K_2O (potassium oxide) have lower abundances than the previous two major elements, with the abundances of Fe_2O_3 ranging from 9.33% in PR 7 to 5.16% in PR 9 and K_2O ranging from 7.22% in PR 4 to 3.16% PR 7. Fe_2O_3 and SiO_2 appear to be positively correlated to each other, with both having similar curves. TiO_2 (titanium dioxide), Na_2O (sodium oxide), MgO (Magnesium oxide), CaO (Calcium oxide), and P_2O_5 (Phosphorus pentoxide) all have curves that are positively correlated with the previously mentioned Al_2O_3 and K_2O, however with much lower percentage abundance. TiO_2 abundance ranges from 2.01% to 0.91%, with Na_2O having a range of 1.29% to 0.65%, following MgO range is 0.79% to 0.21%, CaO ranges from 0.36% to 0.04%, and finally P_2O_5 has a range of 0.23% to 0.05%. MnO (Manganese (II) oxide) doesn't appear to correlate with any of the other major elements and also has the lowest overall abundance, with the percentage being shared by PR 3 and PR 6 at 0.09%.

Focusing on the relationship between the major elements and the DCB, the curves mentioned previously are shown to occur around the DCB. SiO_2, is the major element with the highest abundance; is also one of the two major elements with the most significant variations. The abundance of SiO_2 is shown to drop to its lowest percentage value at PR 4, 47.61%, which coincides with the DCB, and then after PR 5, the sample directly after the DCB, the abundance of this element quickly increases in the younger sediments in the Carboniferous. Al_2O_3 is the second of the major elements with the highest percentage abundance and, as discussed earlier, has a strong inverse correlation with SiO_2, which, as seen in Graph 5, almost perfectly mirrors the other. Being inversely correlated with SiO_2 means that instead of decreasing near the DCB, Al_2O_3 abundance increases around the DCB, with Al_2O_3 increasing from 27.30% in the oldest

Devonian sediments to 34.78% in PR 4. Also, like with SiO_2, as the ages of the samples get young after the DCB, the abundance of Al_2O_3 has a decreasing trend. Fe_2O_3 correlated with SiO_2 means that Fe_2O_3 abundance decreases when looking at the samples. However, there is much less variation with the abundance of Fe_2O_3 than SiO_2. This lack of extreme variation in the abundance of Fe_2O_3 can be best seen in the four samples around the DCB in Graph 5, with PR 3 and PR 4 being from older sediments in the Devonian period and then from the other side of the DCB with PR 5 and RR 6 of the younger Carboniferous sediments. Similar to Fe_2O_3 with SiO_2, K_2O has a positive correlation with Al_2O_3, with Graph 5 showing this correlation to have similar times of rise and decline of abundance to Al_2O_3 around and during the DCB. The major elements of TiO_2, Na_2O, MgO, CaO, and P_2O_5, as talked about in the previous paragraph, are positively correlated, which means that around the time of the DCB, there is a rise in the abundance in these elements. MnO does not show the same rise or decline around the DCB that the other major elements, with an increase in abundance in PR 3 and PR 6.

Age	Sample	SiO_2	Al_2O_3	Fe_2O_3	MnO	MgO	CaO	Na_2O	K_2O	TiO_2	P_2O_5
Carboniferous	PR9	67.21	21.19	5.16	0.03	0.32	0.04	0.82	4.13	1.05	0.05
↓	PR8	68.25	18.77	6.91	0.08	0.32	0.04	0.98	3.61	0.98	0.05
↓	PR7	66.14	19.34	9.33	0.05	0.21	0.11	0.65	3.16	0.91	0.11
↓	PR6	65.03	22.02	5.85	0.09	0.30	0.19	1.05	3.93	1.37	0.18
DCB	PR5	50.11	32.75	5.88	0.07	0.79	0.25	1.29	6.68	2.01	0.17
DCB	PR4	47.61	34.78	6.11	0.08	0.51	0.25	1.28	7.22	1.94	0.23
↑	PR3	52.33	31.69	5.78	0.09	0.60	0.36	1.04	6.39	1.53	0.20
↑	PR2	58.60	26.28	7.60	0.06	0.30	0.03	1.01	4.67	1.37	0.08
Devonian	PR1	59.30	27.30	5.27	0.06	0.37	0.04	1.25	4.81	1.53	0.08

Table 7: Table of the abundances of Major Elements observed in the Southern Outcrop organized by oldest samples at the bottom and young samples at the top.

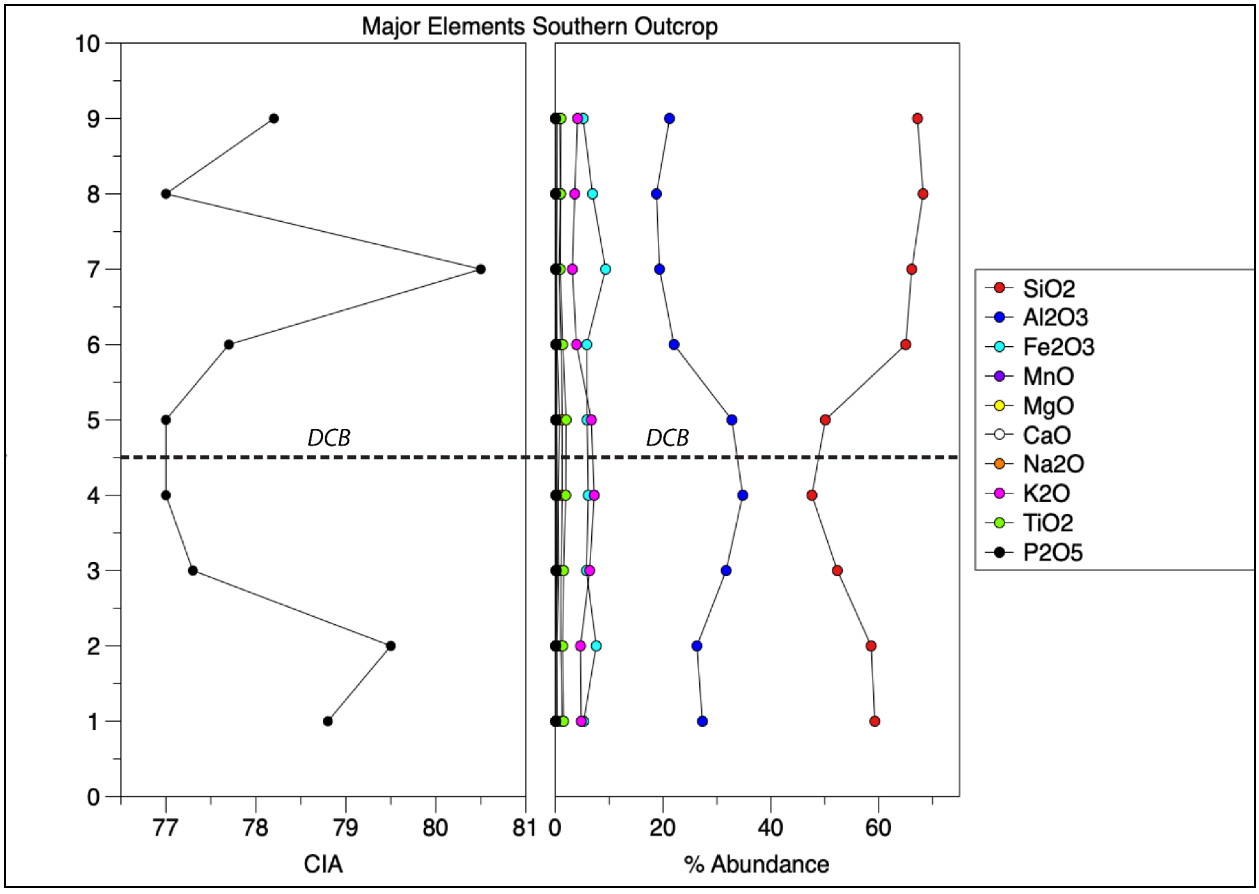

Graph 5: Graphical representation of Major Element abundances shown alongside the CIA values for the Southern Outcrop.

4.3.b Northern Outcrop

Analyzing Graph 6 and Table 8, one of the first trends that can be noticed is that the abundances of the major elements in the Northern Outcrops do not have the same variation in the most abundant major elements of SiO_2 and Al_2O_3 as the Southern Outcrop had. SiO_2 ranges from 58.69 to 71.90, which appears consecutively in PR 13 and PR 14 directly before the DCB, with Al_2O_3 having its range from 17.12 in PR 14 to 25.96 in PR 16. The abundance of Fe_2O_3 appears to have a decent amount of variation relative to the Southern Outcrop, with the lowest percentage for Fe_2O_3 being 0.51, seen in PR 20, and the highest being 11.54 in PR10. K_2O, similar to SiO_2 and Al_2O_3, doesn't seem to have much variation in its abundance, with the range for K_2O being from 3.38 in PR 14 to 5.42 in PR 16. Like in the Southern Outcrop, the major elements TiO_2, Na_2O, MgO, CaO, P_2O_5, and MnO have, on average, lower percentage abundances than the other major elements, with all of these elements having abundances that are lower than 2%, with CaO

having the lowest average and MnO having the lowest percentage overall with PR 17, PR 19, and PR 20 having a percent abundance of 0 for MnO.

Some patterns can be seen in the relationship between the major elements of the Northern Outcrop and the DCB. The SiO_2 percent abundance shows an increase around the time of the DCB, with a jump from an abundance of 58.69 in PR 13 to 71.90 in PR 14, which coincides around the same time to the DCB. This jump in the abundance of SiO_2 at the DCB does decrease after this event, though SiO_2 is somewhat more abundant in the Carboniferous than in the previous Devonian. Al_2O_3 suffers a decline in abundance right around the DCB, which has the lowest abundances for Al_2O_3 in the Northern Outcrop, which can be seen better in Table 8. The decline in the abundance of Al_2O_3 is shown to quickly recover in the Carboniferous, with the abundances of this period often exceeding that of abundances seen before the DCB. Looking at both Graph 6 and Table 8, there isn't much of a pattern of decline and increase for the percent abundance of Fe_2O_3 around the DCB, with a more gradual decline in the abundance in the older samples leading up to the DCB. After the DCB, the abundance for Fe_2O_3 decreases sharply and recovery with no fundamental visible patterns for these changes about the DCB or the other major elements. K_2O shows even fewer changes that could be attributed to the DCB, with abundances for this compound staying relatively constant and only showing a slight trend of increase after the DCB. Another major element that seems to follow a trend of a slight increase in abundance after the DCB is Na_2O, which shows a higher average of abundance after the DCB. In contrast, P_2O_5 shows a mostly decreasing trend in the percentage after the DCB. The other major elements, TiO_2, MgO, CaO, and MnO, do not show trends or patterns in relation to the other major elements or the DCB, Although MnO is shown to be the only major element that has abundances of 0 seen in PR 27, PR 19, and PR 20.

Age	Sample	SiO_2	Al_2O_3	Fe_2O_3	MnO	MgO	CaO	Na_2O	K_2O	TiO_2	P_2O_5
Carboniferous	PR19	67.50	23.89	1.87	0	0.27	0.04	0.97	4.25	1.15	0.05
↓	PR18	63.72	23.07	6.65	0.05	0.32	0.05	0.83	4.24	1.01	0.05
↓	PR17	66.78	22.53	4.11	0	0.24	0.03	0.87	4.30	1.10	0.05
↓	PR16	59.05	25.96	6.43	0.13	0.40	0.05	1.06	5.42	1.41	0.09
↓	PR20	69.69	23.13	0.51	0	0.23	0.03	0.90	4.37	1.10	0.04
DCB	PR15	65.96	19.83	7.40	0.18	0.32	0.05	0.74	4.26	1.16	0.08
DCB	PR14	71.90	17.12	5.45	0.05	0.24	0.04	0.77	3.38	0.97	0.08
↑	PR13	58.69	22.52	11.24	0.51	0.40	0.07	0.88	4.22	1.35	0.13
↑	PR12	62.93	22.89	7.15	0.14	0.29	0.10	0.84	4.20	1.35	0.11
↑	PR11	64.89	20.60	8.00	0.09	0.32	0.08	0.84	3.76	1.26	0.17
Devonian	PR10	59.30	22.73	11.54	0.05	0.43	0.05	0.82	4.01	1.03	0.05

Table 8: Table of the abundance of Major Elements observed in the Northern Outcrop organized in stratigraphic order.

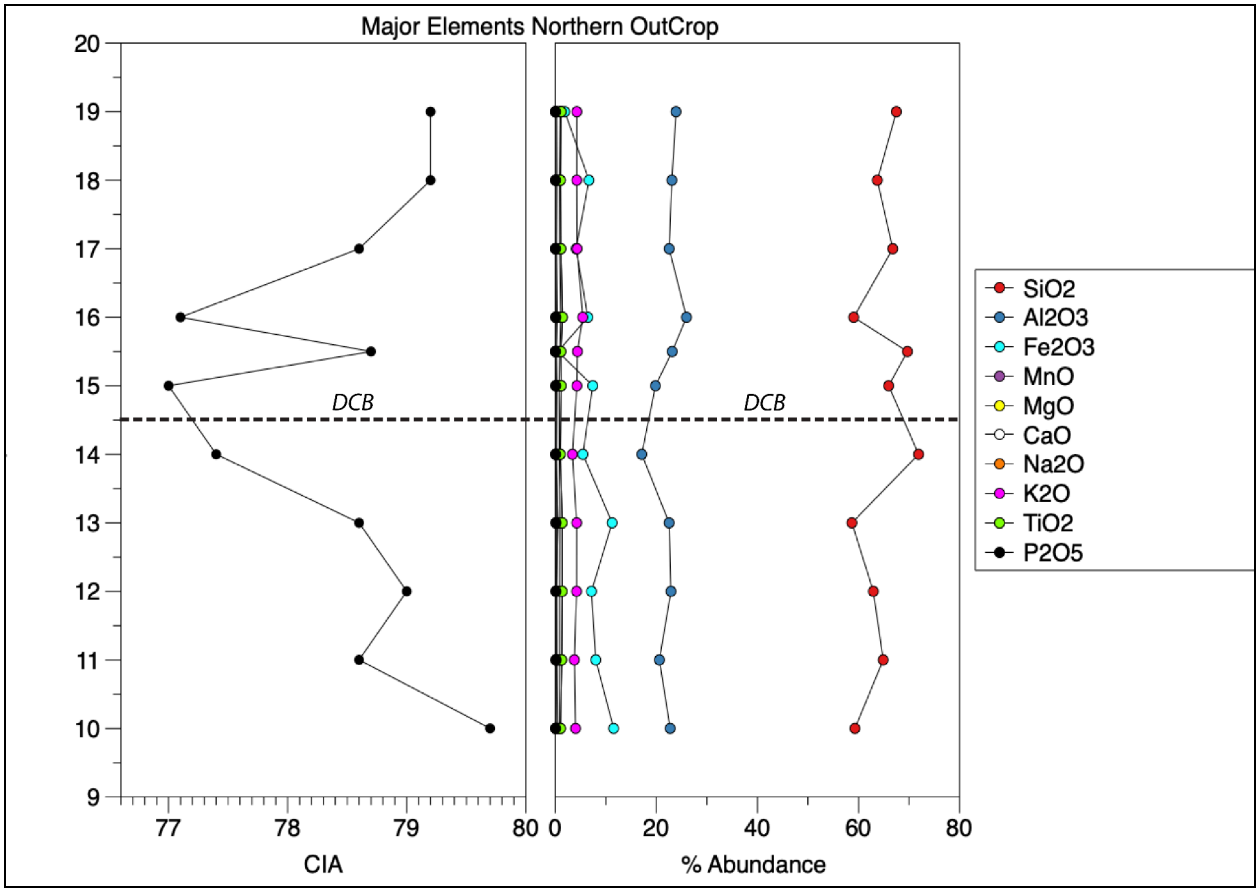

Graph 6: Graphical representation of Major Element abundances shown alongside the CIA values for the Northern Outcrop.

4. Discussion

This thesis aimed to determine if there is evidence of anoxic events in the stratigraphic sequence associated with the Devonian-Carboniferous Boundary (DCB) in the South Portuguese Zone. The geochemical and sedimentological results attained from the Southern and Northern outcrops of the Pedra Ruiva Section in this study indicate that the End Devonian, DCB, and Early Carboniferous were a time of environmental changes in the South Portuguese Zone. In both outcrops, changes in the CIA value are shown to coincide with the time of the DCB, with both showing drops in the values, which indicates a change in the extent of chemical weathering that occurred during the time of the DCB (Nesbitt & Young, 1982). The analysis of the other variables used in this thesis also shows changes occurring that coincide with the DCB in the two outcrops. The Southern Outcrop shows a significant increase in the heavy metals vanadium and

chromium as well as an increase in the abundance of the major elements of Al_2O_3 and K_2O that correlated with the DCB. Other smaller increases of the other major elements of TiO_2, Na_2O, MgO, CaO, and P_2O_5 also occur at this time. A decrease in the ratio of V/Cr leading up to the DCB and the major elements SiO_2 and Fe_2O_3 are also shown coinciding with the DCB in the Southern Outcrop. The analysis of the Northern Outcrop shows sharp increases and decreases in the heavy metals Nickel and Cobalt in the samples before and after the DCB. The Northern Outcrop also shows an increase in the ratio V/Cr just before the DCB occurred and an increase in the ratio V/(V+Ni) just after the DCB. The percentage of major elements for the Northern Outcrop indicate a decrease in the abundance of Al_2O_3 and an increase in the abundance of SiO_2 around the time of the DCB. Other major elements in the Northern Outcrop show general increasing trends, such as K_2O, and decreasing trends, such as Fe_2O_3, occurring after the DCB.

4.1 Sedimentology

Before discussing the sample analysis results on the Southern and Northern Outcrops, a look into the lithology of the two outcrops, which can be seen in Figure 3 as well as Graphs 1 through 4, will help add context to the results discussed further. Looking at the lithology of the Southern Outcrop, there is an evident change in the lithology during the Devonian before the DCB and during the Carboniferous after the DCB. Before the DCB in the Devonian period, the lithology of the Southern Outcrop consisted mostly of claystones interbedded with sandstones. After the DCB in the Carboniferous, the lithology of the Southern Outcrop changed dramatically from being mostly made up of claystones to being almost entirely sandstones made up of sandy sediments that vary in grain size. This change in lithology from the smaller and finer sediments that make up claystones to the larger and coarser sediments that make up sandstones may be indicative of a change in the sea level of the Southern Outcrop. This is due to how the water transports sediments in marine environments, with coarser sediments needing more energy and power in order for them to be transported and deposited. In marine settings, shallower water is subject to stronger currents closer to the surface, and tidal currents are present in near-shore/intertidal settings. These tides and currents provide the power to move and deposit coarse-grained sediments; however, in deeper waters, this influence is lessened, which causes only smaller, fine-grained sediments to be moved and deposited. This provides evidence that the

change in the lithology of the Southern Outcrop that occurs after the DCB may be due to a fall in sea level (Collinson et al., 2006; Nichols, 1999).

The Northern Outcrop does not show the same pattern within the lithology, with the lithology of this outcrop showing the same pattern from both before and immediately after the DCB. The vertical arrangement of the lithologies is shown to be similar to the Southern Outcrop before the DCB occurred, showing claystone-dominated sediments with sandstone incursions. Based on the earlier discussed Southern Outcrop, this may indicate the depth of the environment in which these sediments were deposited, with the finer claystone sediments indicating that this outcrop was located in deeper waters than the previous outcrop. This could likely mean that the Northern Outcrop was more offshore than the Southern Outcrop, therefore, under less influence from tidal and wave currents. The Northern Outcrop continues this same vertical pattern of the distribution of the beds until just over 12.5 m depth in the log, to just under 17.5 m depth. At this point, the lithology changes completely to sandstones. The change in lithology in this part of the succession, like in the Southern Outcrop, is likely an indicator of sea level fall; however, due to the Northern Outcrop having a deeper and less dynamic depositional environment, most likely being further offshore, this is not as extreme as in the Southern Outcrop (Collinson et al., 1999).

Besides using the bed lithologies of the two outcrops, the sedimentary structures found in them can also be used to make inferences about the depositional conditions and environments in which these sediments were deposited. Figure 3 shows the logs and key for the lithology and sedimentary structures of the Northern and Southern outcrops generated by the Sedlog application used to create the sedimentary logs in Figure 3 and Graphs 1 through 4. The key and the graphs show that before the DCB in the Southern and Northern outcrops, the environment appeared relatively stable, with evidence of both current ripple and wave ripple cross-lamination. The wave ripple cross-lamination most likely occurred due to ripples created by wave action on the sediments. Meanwhile, the current ripple lamination observed results from unidirectional water currents acting on the sediments (Collinson et al., 2006; Nichols, 1999). The presence of wave ripples in the Southern Outcrop helps to support the conclusion that this outcrop represents a shallower depositional environment, while the Northern Outcrop corresponds to a deeper environment that did not show the presence of wave ripples. Since wave ripples are caused by wave action at the ocean's surface, the impact of wave action on sediments will lessen and eventually disappear as the depth increases (Nichols, 1999). Shifting the focus to sedimentary

structures only present in the Northern Outcrop, there is evidence of minor bioturbation, which is a term used to describe trace fossils in sediments that represent the movement of living organisms, with these structures in the outcrop being an indication of the presence of oxygenated sediments (Taylor & Goldring, 1993; Nichols, 1999; Kristensen et al., 2012).

After the DCB in the Southern Outcrop and the change from mostly claystones to sandstones, there is a much more diverse number of sedimentary structures. The first of these new sedimentary structures is horizontal parallel lamination, which occurs directly after the DCB and occurs when sediments are deposited by fast-flowing currents in the upper flow regime (Bridge, 2020; Collinson et al., 2006). This sedimentary structure is the most common one observed in the Southern Outcrop after the DCB. Another sedimentary structure observed in this outcrop is planar cross-bedding, formed by the movement of submerged dune bedforms (Collinson et al., 2006; Nichols, 1999). The next form of cross-bedding seen in the outcrops is herring-bone cross-bedding, associated with nearshore subtidal zones. As such, the presence of this particular form is another indicator of the Southern Outcrop being a shallow water depositional setting (Collinson et al., 2006). The final sedimentary structure seen in the Southern Outcrop is known as swaley cross-stratification, which is a structure that is also associated with shallow water depositional settings, with this particular structure believed to be formed by vigorous and complex wave activity caused by storm activity in the area (Collinson et al., 2006).

The stratigraphic sequence of the Northern Outcrop differs from the Southern Outcrop in that the sedimentary structures observed before and after the DCB remain unchanged until ca.12.5 m in the log. As mentioned, the Northern Outcrop had evidence of both current ripple lamination and minor bioturbation, with these sedimentary structures remaining after the DCB. The presence of these sedimentary structures both before and after the DCB indicates that this environment remained relatively stable when compared with the Southern Outcrop, as well as being an indicator that the Northern Outcrop was located in deeper offshore waters. The presence of bioturbation itself is a strong indicator of the stable environment, as this is evidence of marine organisms living in the outcrop both before and after the DCB (Taylor & Goldring, 1993; Kristensen et al., 2012). As mentioned before, the patterns found in the lithology of the Northern Outcrop remain the same until just above 12.5 m. At this point, the lithology changes from claystones sandstone intercalations to only being composed completely of sandstones until just below 17.5 m. This indicates a drastic change in the environment of the Northern Outcrop, which

is further supported by the presence of parallel laminations and two types of cross-bedding in this particular area of the outcrop, planar and herring-bone cross bedding. As mentioned when discussing the Southern Outcrop's sedimentary structures, these forms of lamination and cross-bedding are indicative of fast-flowing currents and shallow water deposition of sediments (Bridge, 2020; Collinson et al., 2006). As a result, these changes in the lithology of the Northern Outcrop appear to be indicative of a drop in the sea level at this time, with stronger impacts of currents and tides on the sediment regimes of the area.

One last sedimentary feature of the South Portuguese Zone that should be discussed is the presence of the five erosional base boundaries found in the Southern Outcrop. These base boundaries represent powerful erosional events that remove large portions of already deposited sediments and result in non-continuous time stratigraphic succession. With this removal of sediments, the sedimentary record that was recorded in this outcrop is lost and is not represented in the studied sections.

4.2 Chemical Index of Alteration

Looking at the Southern and Northern Outcrop's results, there are some obvious patterns in data regarding the DCB. These patterns indicate that changes were happening during that time, in the environment. As previously mentioned, the CIA value indicates the degree of chemical weathering that occurred in the surrounding continental areas during the formation of sediment layers (Nesbitt & Young, 1982). CIA values of 60 to 80 show moderate amounts of chemical weathering and values above 80 show high amounts of chemical weathering (Ivančič et al., 2024; Hu et al., 2014). Upon analyzing both outcrops, it is evident that most samples exhibit CIA values below 80, suggesting moderate chemical weathering during this period. Both the Southern and Northern Outcrops are shown to consistently stay below the value of 80 with the exception of PR 7. At the occurrence of DCB both outcrops show a decline in CIA values however in both outcrops the values do not drop below 77. This indicates that the moderate level of chemical weathering taking place in the South Portuguese Zone was not heavily impacted by the DCB. Both outcrops stay within values of high 70s with PR 7 of the Southern outcrop. While the change that takes place in the two outcrops is not very large, the CIA values show a slight decrease that coincides with the DCB. A possible cause for this decrease in CIA values of the outcrops may be a result of a cooling trend that occurred at the end of the Devonian which

resulted in a glacial period that continued into the Early Carboniferous period (Brezinski et al., 2008; Isaacson et al., 2008; Streel, 2000). This is due to cooler and drier climates having lower rates of chemical weathering than warmer and wetter climates, however it should be noted that due to the relatively small change in values that are observed in the outcrops the factor alone does not support climate cooling or glaciation.

4.3 Major Element Oxides

The major element oxides for the Southern and Northern outcrops can indicate the rates of weathering that were occurring in the outcrops at the time. The oxides Al_2O_3, CaO, Na_2O, and K_2O were used to calculate the CIA values, so looking at these oxides can further support the observation made in the CIA values. The relatively low abundances of CaO, Na_2O, and K_2O present in both the Southern and Northern outcrops are indicators of higher levels of chemical weathering shown by the CIA values (Nesbitt & Young, 1982). Both outcrops show a negative correlation between the abundance of SiO_2 and that of the oxides used to calculate the CIA value, with the Southern Outcrop showing this correlation the strongest. The negative correlation between SiO_2 and the oxides used to calculate the CIA indicates that the dominant form of weathering occurring at this time was chemical weathering (Jorge et al., 2013). This coincides with CIA values indicating moderate to high amounts of chemical weathering occurring with drops and increases in CIA values correlating with drops and increases in the abundance of SiO_2.

4.4 Heavy Metals

As discussed before, the analysis of heavy metals shows many patterns and relationships in both the Southern and Northern Outcrops. As with the CIA values, many of the patterns seen occur around the time of the DCB, which can also allow for the observation of relations with the CIA value. Like with the other variables analyzed, the presence and abundance of the heavy metals indicate certain environmental conditions that could have occurred when the sediments were deposited. For example, heavy metal V can be associated with anoxic conditions and organic sequestration (Emerson & Huested, 1991; Li et al., 2022). Because of this, V and the other heavy metals can be used as environmental proxies that can give insight into the conditions of the South Portuguese Zone during the DCB.

4.4.a Southern Outcrop

The heavy metals V and Cr in the Southern Outcrop are the best examples of these heavy metals being heavily correlated with the DCB and CIA values. From samples PR 3 to PR 4, there is a sharp increase in the abundance of both metals in conjunction with the occurrence of the DBC, with V increasing from 182 ppm to 211 ppm and Cr from 130 ppm to 170 ppm. Both these elements then sharply decline in value at sample 6 after the DCB, with this decline also coinciding with an increase in chemical weathering as indicated by the CIA value. Interestingly, samples 1 and 2 seem to suggest that before the DCB occurred, higher rates of chemical weathering did not have a negative impact on the abundance of V, which may be an indication of other factors impacting V. One of these different factors that may be impacting the abundance of V in the Southern Outcrop may be seen in the sedimentology of this outcrop as after the DCB there is a dramatic shift in the sedimentology from the Devonian into the Carboniferous. Based on the analysis of the sedimentology of the Southern Outcrop, we see that the sedimentology changes from relatively stable claystone-dominated sediments to much more dynamic sandstone-dominated sediments. As discussed in the Sedimentology section earlier, the Southern Outcrop shows evidence that the area was subjected to sea level fall, resulting in the outcrop sediments being more impacted by shallow water tidal currents, wave motion, and storms. As these factors impact the deposition of sediments in the area this may have had an impact on the abundance of V. This change in sedimentology was also responsible, at least in part, for the change in the abundance of Cr, as Cr is more commonly found in claystone sediments (Frank et al., 2020).

As mentioned before, V is sometimes associated with anoxic conditions and organic sequestration so the overall high abundance of this metal in marine sediments may be indicative of lowered oxygen conditions (Emerson & Huested, 1991). The global average of V in the upper continental crust is around 98 ppm, and by looking at the values of V found in the Southern Outcrop, it is clear that throughout most of the outcrop, this element is enriched (Hans Wedepohl, 1995). Cr like V is also often associated with organic matter and has been used to track paleoredox changes with a global average of about 126 ppm (Hans Wedepohl, 1995; Frank et al., 2020). Comparing the global average to what is observed in the outcrop shows that the abundance of Cr falls closely around the global average, with samples adjacent to the DCB

showing some enrichment with values of 160 ppm and 170 ppm. The heavy metal U seems to correlate with the DCB, and the metal shows a spike in abundance around the time of the DCB before decreasing again in abundance after the DCB. This correlation is likely due to U being associated with the rise and drops in V and Cr, as U is related to similar environmental conditions (Algeo & Tribovillard, 2009). Comparing the global average abundance of U, 1.7 ppm, with the values found in the outcrop, shows that U is indeed enriched, with all values above the average and samples adjacent to the DCB having abundances of 6.20 ppm and 6.61 ppm (Hans Wedepohl, 1995). The patterns seen in the heavy metals V, Cr, and U indicate that during the End Devonian, DCB, and Early Carboniferous, these metals were all enriched in the sediments of the environment, especially in those samples adjacent to the occurrence of the DCB. As for the other outcrop, regarding Co, Ni, and Pb metals, there are no strong correlations with the CIA value, the DCB, or the other heavy metals.

4.4.b Northern Outcrop

The Northern Outcrop, like the Southern Outcrop, shows that the metals V and Cr have the highest abundance of heavy metals in the outcrop, although V's overall abundance is lower in the Northern Outcrop. As mentioned previously, there is less correlation between the CIA values and the abundance of the metals V and Cr in this outcrop than is observed in the Southern Outcrop. While these two metals do not show as strong of a correlation with the CIA value or each other in the Northern Outcrop they still share a trend of general increase after the occurrence of the DCB. Interestingly, the metals Co and Ni show a somewhat stronger correlation with the CIA value of the Northern Outcrop, which differs from the Southern Outcrop, which showed little to no correlation between the CIA and these two metals. After the DCB, the abundances of Co and Ni have an inverse correlation with CIA values, which is best seen in the sediments that occurred soon after the DCB. Both Co and Ni show an extreme drop in their abundances at PR 20, with Co showing a drop from 29 ppm to 1 ppm and Ni from 58 ppm to 8 ppm. Co and Ni recover sharply in abundance to 31 ppm and 61 ppm, respectively, coinciding with a drop in the CIA value.

Looking at the global average abundance of Co, 24 ppm, and Ni, 56 ppm, it is shown that the Northern Outcrop samples that show enrichment, occur before the DCB (Hans Wedepohl, 1995). After the DCB, the only samples that show enrichment occur during the major

drops in the CIA values at PR 15 and PR 16. Looking at the abundances of V, Cr, and U for the Northern Outcrop, it is possible to observe that while V and U are enriched like in the Southern Outcrop, Cr is not and is slightly under the global average, ranging from 100 ppm to 120 ppm. Both V and U show overall lower enrichment in the Northern Outcrop compared with the Southern Outcrop and do not show any correlation with the CIA or other metals. As with the Southern Outcrop, the abundance of Pb in the Northern Outcrop does not strongly correlate with the CIA value, the DCB, or the other heavy metals.

4.5 Heavy Metal Ratios

Like the heavy metals discussed before, heavy metal ratios can be used as different environmental proxies to show what environmental conditions were present when the sediments were deposited in a particular area. The ratios used for the thesis of V/Cr, U/Th, and V(V+Ni) are all redox-sensitive ratios and the values of these ratios are being used to help see if there may have been any anoxic or low oxygen events during the DCB (Hatch & Leventhal, 1992; Jones & Manning, 1994; Wang et al., 2016). By using the thresholds for the ratios of V/Cr and U/Th established by Jones & Manning (1994) and the ratio of V(V+Ni) established by Hatch & Leventhal (1992), we can infer whether a sample was deposited in an anoxic or oxygen-rich ecosystem (Riquier et al., 2006). It should be noted that these thresholds cannot be individually used to indicate whether a marine sedimentary layer was deposited in anoxic conditions and must be considered collectively to make a more accurate assessment of the samples and outcrops (Riquier et al., 2006).

4.5.a Southern Outcrop

Looking at the ratio values V/Cr in the Southern Outcrop, as seen in Table 5, the values of this ratio range from 1.10 to 1.58, with the lowest values of 1.10 coinciding with the DCB. For the thresholds of ratio V/Cr to be considered in the anoxic zone, there needs to be a value higher than 4.5, while if the value is lower than 2, it is considered oxic (Jones & Manning, 1994; Riquier et al., 2006). Based on these values of V/Cr seen in Table 5 and the thresholds, this ratio indicates a more oxygen-rich environment for the Southern Outcrop during the DCB. Graph 3 shows a positive correlation between CIA and V/Cr, with both decreasing in value about the DCB and then gradually increasing after the DCB. This correlation may indicate that there may

be a relation to the variables impacting the rate of chemical weathering and causing the decrease in the ratio of V/Cr. Looking at the ratio of U/Th, we use the thresholds for U/Th established by Jones & Manning (1994), which in this case are any values above 1.25 that are considered anoxic, and any values below 0.75 considered oxic (Jones & Manning, 1994; Riquier et al., 2006). Using Table 5 again to look at the U/Th of the Southern Outcrop, the values for this ratio range from 0.20 to 0.26, which would indicate an oxic environment based on U/Th. It should also be noted that U/Th is the most constant of the three ratios used throughout the Southern Outcrop; this could indicate that any changes occurring because of the DCB did not impact the ratio of U/Th. The third ratio, V(V+Ni), will be using the threshold established by Hatch & Leventhal (1992) which indicates that values ranging from 0.54 to 0.82 would be considered anoxic while values below 0.46 should be considered oxic (Hatch & Leventhal, 1992; Riquier et al., 2006). Going back to Table 5, the V(V+Ni) ratio, unlike the previous two ratios, indicates anoxia with a range of 0.69 to 0.84. The range of values for V(V+Ni) falls well within the range established by Hatch & Leventhal (1992), which would be identified as anoxic.

4.5.b Northern Outcrop

Using the same thresholds provided by Riquier et al. (2006) for the ratio V/Cr that was used before for the Northern Outcrop, it appears that this ratio also indicates a more oxygen-rich environment for this outcrop as well, with a range of 1.3 to 1.45 present in this outcrop as seen in Table 6 (Jones & Manning, 1994; Riquier et al., 2006). Like in the Southern Outcrop, the V/Cr ratio of the Northern Outcrop seems to be correlated with the CIA, seen in Graph 4, a value which further supports that the factors impacting the rate of chemical weathering may also be related to values of the V/Cr ratio. Looking at the U/Th ratio values in Table 6, there is a range between 0.16 to 0.22, which puts the values of this ratio within the threshold of U/Th being considered oxic (Jones & Manning, 1994; Riquier et al., 2006). Similar to the Southern Outcrop, the ratio of U/Th for the Northern Outcrop is the most constant of the three ratios analyzed, which may be indicative of the changes occurring around the DCB that did not have an impact on U/Th of the South Portuguese Zone. The ratio V(V+Ni) shows a range of 0.61 to 0.95, which, like in the Southern Outcrop, means that V(V+Ni) falls within the range of being considered anoxic (Hatch & Leventhal, 1992; Riquier et al., 2006). Unlike the Southern Outcrop; however,

the ratio V(V+Ni), like V/Cr, is positively correlated with the CIA value, best seen in the spike in value at Sample PR 20.

Recommendations

The sedimentary environments interpreted for the South Portuguese Zone outcrops indicate shallow siliciclastic marine settings affected by tidal and wave processes. These highly active environments are prone to erosional processes that remove previously deposited sediments, forming a non-continuous time stratigraphic succession. Also, the siliciclastic nature of the DCB at the South Portuguese Zone is not ideal for recording the geochemical proxies used for OAE detection, which are better preserved in time-continuous mud-dominated offshore marine successions. The Southern Outcrop shows evidence of large-scale erosional events occurring shortly after the DCB. This means that with the removal of sediments, due to these events, there are several time hiatuses in this sedimentary record. Geochemical data that can be added to future studies is the organic content of sedimentary rocks.

Safety concerns limited the sample collection process, preventing access to certain areas. If future studies require samples from these areas, these safety concerns must be addressed before beginning sample collection. Climbing and rappelling equipment, along with experienced professionals in these activities, would be recommended for accessing many outcrop areas.

5. Conclusions

The main aim of this exploratory thesis is to determine whether there is evidence of anoxic events in the rock record of the South Portuguese Zone at the Devonian-Carboniferous Boundary. The second goal is to utilize geochemical proxies to systematically document any anoxic events that may be identified. The calculated CIA values indicate a decrease in chemical weathering during the time of the DCB, particularly well represented in the Southern Outcrop. This decrease suggests a cooling climate in the environment of the South Portuguese Zone during the DCB, which is supported by previous studies of this time. The sedimentary facies observed in the Southern Outcrop indicate a sea level at the DCB in this area, likely linked to a

cooling climate suggested by the CIA value. This sea level fall resulted in increased tidal and wave currents, leading to changes in deposition, creating erosion surfaces in the stratigraphic succession. The Northern Outcrop also shows evidence of a sea level fall. However, its succession suggests that it represents more offshore conditions less affected by nearshore wave and tidal processes. Due to the fall in sea levels and the shallower settings within the platform, a more energetic environment has led to the deposition of coarser sandy sediments. The strong mixing from tides and currents has created non-ideal conditions for the preservation of proxies used to detect OAEs. While the presence of heavy metals such as uranium, vanadium, and chromium may indicate anoxic conditions, this could be attributed to intense mixing and replacement resulting from wave and tide action. The ratios of V/(V+Ni) fall within the anoxic threshold, but the ratios of U/Th and V/Cr do not fall within that threshold. These findings do not provide a definitive answer. However, the Tercenas Formation shows a deepening trend towards the north, so it is possible that more definitive data can be gathered from a more northern location where the DCB is preserved.

References

- Algeo, T. J., & Maynard, J. Barry. (2004). Trace-element behavior and redox facies in core shales of Upper Pennsylvanian Kansas-type cyclothems. *Chemical Geology*, *206*(3-4), 289–318. https://doi.org/10.1016/j.chemgeo.2003.12.009
- Algeo, T. J., & Scheckler, S. E. (1998). Terrestrial-marine teleconnections in the Devonian: links between the evolution of land plants, weathering processes, and marine anoxic events. *Philosophical Transactions of the Royal Society of London. Series B: Biological Sciences*, *353*(1365), 113–130. https://doi.org/10.1098/rstb.1998.0195
- Algeo, T. J., & Scheckler, S. E. (2010). Land plant evolution and weathering rate changes in the Devonian. *Journal of Earth Science*, *21*(S1), 75–78. https://doi.org/10.1007/s12583-010-0173-2
- Algeo, T. J., & Tribovillard, N. (2009). Environmental analysis of paleoceanographic systems based on molybdenum–uranium covariation. *Chemical Geology*, *268*(3-4), 211–225. https://doi.org/10.1016/j.chemgeo.2009.09.001
- Aretz, M. (2021). Late Devonian Extinctions. *Encyclopedia of Geology (Second Edition)*, *3*, 628–636. https://doi.org/10.1016/b978-0-12-409548-9.12453-4
- Aretz, M., & Corradini, C. (2021). Global review of the Devonian-Carboniferous Boundary: an introduction. *Palaeobiodiversity and Palaeoenvironments*, *101*(2), 285–293. https://doi.org/10.1007/s12549-021-00499-8
- Begum, T. (2021, May 19). What is mass extinction and are we facing a sixth one? *Natural History Museum, London*. Retrieved from https://www.nhm.ac.uk/discover/what-is-mass-extinction-and-are-we-facing-a-sixth-one.html
- Brezinski, D. K., Cecil, C. B., Skema, V. W., & Stamm, R. (2008). Late Devonian glacial deposits from the eastern United States signal an end of the mid-Paleozoic warm period. *Palaeogeography, Palaeoclimatology, Palaeoecology*, *268*(3-4), 143–151. https://doi.org/10.1016/j.palaeo.2008.03.042
- Bridge, J. S. (2020). Planar and parallel lamination. *Encyclopedia of Earth Science*, 869–872. https://doi.org/10.1007/978-1-4020-3609-5_161
- Caplan, M. L., & Bustin, R. Mark. (1999). Devonian–Carboniferous Hangenberg mass extinction event, widespread organic-rich mudrock and anoxia: causes and consequences. *Palaeogeography,*

Palaeoclimatology, Palaeoecology, *148*(4), 187–207. https://doi.org/10.1016/s0031-0182(98)00218-1

- Caplan, M. L., & Marc Bustin, R. (2001). Palaeoenvironmental and palaeoceanographic controls on black, laminated mudrock deposition: example from Devonian–Carboniferous strata, Alberta, Canada. *Sedimentary Geology*, *145*(1-2), 45–72. https://doi.org/10.1016/s0037-0738(01)00116-6
- Carmichael, S. K., Waters, J. A., Batchelor, C. J., Coleman, D. M., Suttner, T. J., Kido, E., … Chadimová, L. (2016). Climate instability and tipping points in the Late Devonian: Detection of the Hangenberg Event in an open oceanic island arc in the Central Asian Orogenic Belt. *Gondwana Research*, *32*, 213–231. https://doi.org/10.1016/j.gr.2015.02.009
- Chen, B., Chen, J., Qie, W., Huang, P., He, T., Joachimski, M. M., … Algeo, T. J. (2021). Was climatic cooling during the earliest Carboniferous driven by expansion of seed plants? *Earth and Planetary Science Letters*, *565*, 116953. https://doi.org/10.1016/j.epsl.2021.116953
- Collinson, J., Mountney, N., & Thompson, D. (2006). *Sedimentary Structures* (3rd ed.). England: Terra Publishing.
- Domeier, M., & Torsvik, T. H. (2014). Plate tectonics in the late Paleozoic. *Geoscience Frontiers*, *5*(3), 303–350. https://doi.org/10.1016/j.gsf.2014.01.002
- Emerson, S. R., & Huested, S. S. (1991). Ocean anoxia and the concentrations of molybdenum and vanadium in seawater. *Marine Chemistry*, *34*(3-4), 177–196. https://doi.org/10.1016/0304-4203(91)90002-e
- Frank, A. B., Klaebe, R. M., Löhr, S., Xu, L., & Frei, R. (2020). Chromium isotope composition of organic-rich marine sediments and their mineral phases and implications for using black shales as a paleoredox archive. *Geochimica et Cosmochimica Acta*, *270*, 338–359. https://doi.org/10.1016/j.gca.2019.11.035
- G. J. Demaison (2), G. T. Moore (3). (1980). Anoxic Environments and Oil Source Bed Genesis. *AAPG Bulletin*, *64*(8). https://doi.org/10.1306/2f91945e-16ce-11d7-8645000102c1865d
- Golonka, J., Porębski, S., Barmuta, J., Papiernik, B., Bębenek, S., Barmuta, M., … Słomka, T. (2019). Palaeozoic palaeogeography of the East European Craton (Poland) in the framework of global plate tectonics. *Annales Societatis Geologorum Poloniae*. https://doi.org/10.14241/asgp.2019.16

- Handoh, I. C., & Lenton, T. M. (2003). Periodic mid-Cretaceous oceanic anoxic events linked by oscillations of the phosphorus and oxygen biogeochemical cycles. *Global Biogeochemical Cycles*, *17*(4), n/a-n/a. https://doi.org/10.1029/2003gb002039
- Hans Wedepohl, K. (1995). The composition of the continental crust. *Geochimica et Cosmochimica Acta*, *59*(7), 1217–1232. https://doi.org/10.1016/0016-7037(95)00038-2
- Hatch, J. R., & Leventhal, J. S. (1992). Relationship between inferred redox potential of the depositional environment and geochemistry of the Upper Pennsylvanian (Missourian) Stark Shale Member of the Dennis Limestone, Wabaunsee County, Kansas, U.S.A. *Chemical Geology*, *99*(1-3), 65–82. https://doi.org/10.1016/0009-2541(92)90031-y
- Herrmann, A. D., Haupt, B. J., Patzkowsky, M. E., Seidov, D., & Slingerland, R. L. (2004). Response of Late Ordovician paleoceanography to changes in sea level, continental drift, and atmospheric pCO2: potential causes for long-term cooling and glaciation. *Palaeogeography, Palaeoclimatology, Palaeoecology*, *210*(2-4), 385–401. https://doi.org/10.1016/j.palaeo.2004.02.034
- Hu, J., Li, Q., Fang, N., Yang, J., & Ge, D. (2014). Geochemistry characteristics of the Low Permian sedimentary rocks from central uplift zone, Qiangtang Basin, Tibet: insights into source-area weathering, provenance, recycling, and tectonic setting. *Arabian Journal of Geosciences*, *8*(8), 5373–5388. https://doi.org/10.1007/s12517-014-1583-8
- Isaacson, P. E., Díaz-Martínez, E., Grader, G. W., Kalvoda, J., Babek, O., & Devuyst, F. X. (2008). Late Devonian–earliest Mississippian glaciation in Gondwanaland and its biogeographic consequences. *Palaeogeography, Palaeoclimatology, Palaeoecology*, *268*(3), 126–142. https://doi.org/10.1016/j.palaeo.2008.03.047
- Ivančič, K., Rok Brajkovič, & Vrabec, M. (2024). Geochemical and Mineralogical Approaches in Unraveling Paleoweathering, Provenance, and Tectonic Setting of the Clastic Sedimentary Succession (Western Central Paratethys). *Applied Sciences*, *14*(2), 537–537. https://doi.org/10.3390/app14020537
- Joachimski, M. M., Breisig, S., Buggisch, W., Talent, J. A., Mawson, R., Gereke, M., … Weddige, K. (2009). Devonian climate and reef evolution: Insights from oxygen isotopes in apatite. *Earth and Planetary Science Letters*, *284*(3-4), 599–609.

https://doi.org/10.1016/j.epsl.2009.05.028
- Joachimski, M. M., & Buggisch, W. (2002). Conodont apatite δ18O signatures indicate climatic cooling as a trigger of the Late Devonian mass extinction. *Geology*, *30*(8), 711. https://doi.org/10.1130/0091-7613(2002)030%3C0711:caosic%3E2.0.co;2
- Jones, B., & Manning, D. A. C. (1994). Comparison of geochemical indices used for the interpretation of palaeoredox conditions in ancient mudstones. *Chemical Geology*, *111*(1-4), 111–129. https://doi.org/10.1016/0009-2541(94)90085-x
- Jorge, R. C. G. S., Fernandes, P., Rodrigues, B., Pereira, Z., & Oliveira, J. T. (2013). Geochemistry and provenance of the Carboniferous Baixo Alentejo Flysch Group, South Portuguese Zone. *Sedimentary Geology*, *284-285*, 133–148. https://doi.org/10.1016/j.sedgeo.2012.12.005
- Kaiser, S. I., Steuber, T., Becker, R. S., & Joachimski, M. M. (2006). Geochemical evidence for major environmental change at the Devonian–Carboniferous boundary in the Carnic Alps and the Rhenish Massif. *Palaeogeography, Palaeoclimatology, Palaeoecology*, *240*(1-2), 146–160. https://doi.org/10.1016/j.palaeo.2006.03.048
- Klinkhammer, G. P., & Palmer, M. A. (1991). Uranium in the oceans: Where it goes and why. *Geochimica et Cosmochimica Acta*, *55*(7), 1799–1806. https://doi.org/10.1016/0016-7037(91)90024-y
- Krencker, F.-N., Lindström, S., & Bodin, S. (2019). A major sea-level drop briefly precedes the Toarcian oceanic anoxic event: implication for Early Jurassic climate and carbon cycle. *Scientific Reports*, *9*(1). https://doi.org/10.1038/s41598-019-48956-x
- Kristensen, E., Penha-Lopes, G., Delefosse, M., Valdemarsen, T., Quintana, C., & Banta, G. (2012). What is bioturbation? The need for a precise definition for fauna in aquatic sciences. *Marine Ecology Progress Series*, *446*, 285–302. https://doi.org/10.3354/meps09506
- Li, S., Wignall, P. B., Poulton, S. W., Hedhli, M., & Grasby, S. E. (2022). Carbonate shutdown, phosphogenesis and the variable style of marine anoxia in the late Famennian (Late Devonian) in western Laurentia. *Palaeogeography, Palaeoclimatology, Palaeoecology*, *589*, 110835. https://doi.org/10.1016/j.palaeo.2022.110835
- Liu, J., Algeo, T. J., Qie, W., & Saltzman, M. R. (2019). Intensified oceanic circulation during Early Carboniferous cooling events: Evidence from carbon and nitrogen isotopes. *Palaeogeography,*

Palaeoclimatology, Palaeoecology, *531*, 108962. https://doi.org/10.1016/j.palaeo.2018.10.021
- Millero, F. J. (2000). Redox Processes in Anoxic Waters. *Chemical Processes in Marine Environments*, 91–123. https://doi.org/10.1007/978-3-662-04207-6_5
- Montoya-Pino, C., Weyer, S., Anbar, A. D., Pross, J., Oschmann, W., van de Schootbrugge, B., & Arz, H. W. (2010). Global enhancement of ocean anoxia during Oceanic Anoxic Event 2: A quantitative approach using U isotopes. *Geology*, *38*(4), 315–318. https://doi.org/10.1130/g30652.1
- Nance, R. D., Gutiérrez-Alonso, G., Keppie, J. D., Linnemann, U., Murphy, J. B., Quesada, C., … Woodcock, N. H. (2012). A brief history of the Rheic Ocean. *Geoscience Frontiers*, *3*(2), 125–135. https://doi.org/10.1016/j.gsf.2011.11.008
- Nasa. (2019). Climate Variability | Science Mission Directorate. Retrieved from Nasa.gov website: https://science.nasa.gov/earth-science/oceanography/ocean-earth-system/climate-variability
- Nesbitt, H. W., & Young, G. M. (1982). Early Proterozoic climates and plate motions inferred from major element chemistry of lutites. *Nature*, *299*(5885), 715–717. https://doi.org/10.1038/299715a0
- Nichols, G. (1999). *Sedimentology & Stratigraphy* (1st ed., pp. 180–193). Wiley Blackwell.
- Oliveira, J. T. (1990). Stratigraphy and Synsedimentary Tectonism. In *Pre-Mesozoic Geology of Iberia* (pp. 334–347). Berlin, Heidelberg: Springer Berlin Heidelberg.
- Oliveira, J. T., Fernandes, P., Pereira, Z., & Borges, M. (2009). CIMP Faro'09: II Joint Meeting of Spores-Pollen and Acritarch Subcommissions. Palynostratigraphic contributions to the Southwest Portugal and Algarve Basin Geology, Portugal: Post Meeting Field-Trip, 23-24 September 2009. *CIMP Faro'09: II Joint Meeting of Spores-Pollen and Acritarch Subcommissions*.
- Ostrander, C. M., Owens, J. D., & Nielsen, S. G. (2017). Constraining the rate of oceanic deoxygenation leading up to a Cretaceous Oceanic Anoxic Event (OAE-2: ~94 Ma). *Science Advances*, *3*(8), e1701020. https://doi.org/10.1126/sciadv.1701020
- Pereira, Z. (1997). *Palinologia e petrologia orgânica do Sector SW da Zone Sul Portuguesa* (PhD Thesis; p. 268). Fac. Ciências da Universidade do Porto.
- Pinckney, J. L., Paerl, H. W., Tester, P., & Richardson, T. L. (2001). The Role of Nutrient Loading and Eutrophication in Estuarine Ecology. *Environmental Health Perspectives*, *109*, 699. https://doi.org/10.2307/3454916

- Riquier, L., Tribovillard, N., Averbuch, O., Devleeschouwer, X., & Riboulleau, A. (2006). The Late Frasnian Kellwasser horizons of the Harz Mountains (Germany): Two oxygen-deficient periods resulting from different mechanisms. *Chemical Geology*, *233*(1-2), 137–155. https://doi.org/10.1016/j.chemgeo.2006.02.021
- Rollinson, H. R., & Pease, V. (2021). *Using geochemical data : to understand geological processes* (pp. 49–53). Cambridge, Uk ; New York, Ny: Cambridge University Press.
- Rue, E. L., Smith, G. J., Cutter, G. A., & Bruland, K. W. (1997). The response of trace element redox couples to suboxic conditions in the water column. *Deep Sea Research Part I: Oceanographic Research Papers*, *44*(1), 113–134. https://doi.org/10.1016/s0967-0637(96)00088-x
- Sallan, L. C., & Coates, M. I. (2010). End-Devonian extinction and a bottleneck in the early evolution of modern jawed vertebrates. *Proceedings of the National Academy of Sciences*, *107*(22), 10131–10135. https://doi.org/10.1073/pnas.0914000107
- Sepkoski, J. J. (1996). Patterns of Phanerozoic Extinction: a Perspective from Global Data Bases. *Global Events and Event Stratigraphy in the Phanerozoic*, 35–51. https://doi.org/10.1007/978-3-642-79634-0_4
- Singh, B., Singh, S., & Bhan, U. (2022). Oceanic anoxic events in the Earth's geological history and signature of such event in the Paleocene-Eocene Himalayan foreland basin sediment records of NW Himalaya, India. *Arabian Journal of Geosciences*, *15*(3). https://doi.org/10.1007/s12517-021-09180-y
- Smart, M. S., Filippelli, G., Gilhooly III, W. P., Marshall, J. E. A., & Whiteside, J. H. (2022). Enhanced terrestrial nutrient release during the Devonian emergence and expansion of forests: Evidence from lacustrine phosphorus and geochemical records. *GSA Bulletin*. https://doi.org/10.1130/b36384.1
- Stanford Earth Staff. (2020, December 9). The science behind extinction. Retrieved January 30, 2023, from Stanford Earth website: https://earth.stanford.edu/news/science-behind-extinction#:~:text=Scientists%20who%20study%20past%20extinction
- Streel, M. (2000). Late Frasnian–Famennian climates based on palynomorph analyses and the question of the Late Devonian glaciations. *Earth-Science Reviews*, *52*(1-3), 121–173. https://doi.org/10.1016/s0012-8252(00)00026-x
- Taylor, A. M., & Goldring, R. (1993). Description and analysis of bioturbation and ichnofabric. *Journal*

of the Geological Society, *150*(1), 141–148. https://doi.org/10.1144/gsjgs.150.1.0141

- Tsandev, I., & Slomp, C. P. (2009). Modeling phosphorus cycling and carbon burial during Cretaceous Oceanic Anoxic Events. *Earth and Planetary Science Letters*, *286*(1-2), 71–79. https://doi.org/10.1016/j.epsl.2009.06.016
- Ullmann, C. V., Thibault, N., Ruhl, M., Hesselbo, S. P., & Korte, C. (2014). Effect of a Jurassic oceanic anoxic event on belemnite ecology and evolution. *Proceedings of the National Academy of Sciences*, *111*(28), 10073–10076. https://doi.org/10.1073/pnas.1320156111
- Wang, S., Dong, D., Wang, Y., Li, X., Huang, J., & Guan, Q. (2016). Sedimentary geochemical proxies for paleoenvironment interpretation of organic-rich shale: A case study of the Lower Silurian Longmaxi Formation, Southern Sichuan Basin, China. *Journal of Natural Gas Science and Engineering*, *28*, 691–699. https://doi.org/10.1016/j.jngse.2015.11.045
- Water Resources . (2019). Nutrients and Eutrophication. Retrieved from Usgs.gov website: https://www.usgs.gov/mission-areas/water-resources/science/nutrients-and-eutrophication

Appendix

Quality Analysis ... **Actlabs** *Innovative Technologies*

Report No.: A23-04529
Report Date: 19-Apr-23
Date Submitted: 04-Apr-23
Your Reference:

Universidade do Algarve
8005-139 FARO
FARO
Portugal

ATTN: PAULO FERNANDES

CERTIFICATE OF ANALYSIS

21 Pulp samples were submitted for analysis.

The following analytical package(s) were requested:		Testing Date:
4B-INAA(Lithores)	QOP INAAGEO (INAA)	2023-04-18 11:55:12
4LITHORES + 4B1 (11+)	QOP WRA/ QOP WRA 4B2/QOP Total (/Major/Trace Elements Fusion ICPOES/ICPMS/Total Digestion ICPOES)	2023-04-11 13:45:16

REPORT **A23-04529**

Notes:

Values which exceed the upper limit should be assayed for most accurate values.

We recommend using option 4B1 for accurate levels of the base metals Cu, Pb, Zn, Ni and Ag. Option 4B-INAA for As, Sb, high W >100ppm, Cr >1000ppm and Sn >50ppm by Code 5D. Values for these elements provided by Fusion ICP/MS, are order of magnitude only and are provided for general information. Mineralized samples should have the Quant option selected or request assays for values which exceed the range of option 4B1. Total includes all elements in % oxide to the left of total. Zr is now being reported from FUS-ICP instead of FUS-MS.

SCC Accredited LAB
LAB Accrédité CCN
LabID: 266

CERTIFIED BY:

Mark Vandergeest
Quality Control Coordinator

ACTIVATION LABORATORIES LTD.
41 Bittern Street, Ancaster, Ontario, Canada, L9G 4V5
TELEPHONE +905 648-9611 or +1.888.228.5227 FAX +1.905.648.9613
E-MAIL Ancaster@actlabs.com ACTLABS GROUP WEBSITE www.actlabs.com

Results **Activation Laboratories Ltd.** **Report: A23-04529**

Analyte Symbol	Au	As	Br	Cr	Ir	Sc	Se	Sb	Mass	SiO2	Al2O3	Fe2O3(T)	MnO	MgO	CaO	Na2O	K2O	TiO2	P2O5	LOI	Total	Sc	Be
Unit Symbol	ppb	ppm	ppm	ppm	ppb	ppm	ppm	ppm	g	%	%	%	%	%	%	%	%	%	%	%	%	ppm	ppm
Lower Limit	2	0.5	0.5	5	5	0.1	3	0.2		0.01	0.01	0.01	0.005	0.01	0.01	0.01	0.01	0.001	0.01		0.01	1	1
Method Code	INAA	INAA	INAA	INAA	INAA	INAA	INAA	INAA	INAA	FUS-ICP	FUS-ICP	FUS-ICP	FUS-ICP	FUS-ICP	FUS-ICP	FUS-ICP	FUS-ICP	FUS-ICP	FUS-ICP	GRAV	FUS-ICP	FUS-ICP	FUS-ICP
PR1	< 2	28.6	6.3	139	< 5	22.5	< 3	2.8	7.22	54.73	25.19	4.86	0.051	0.34	0.04	1.15	4.44	1.415	0.07	5.91	98.20	24	5
PR2	5	77.5	6.9	142	< 5	22.2	< 3	2.5	6.14	53.94	24.19	7.00	0.055	0.28	0.03	0.93	4.30	1.260	0.07	6.39	98.45	23	4
PR3	< 2	23.8	3.0	155	< 5	25.2	< 3	2.0	6.41	48.29	29.25	5.33	0.084	0.55	0.33	0.96	5.90	1.414	0.18	6.55	98.83	26	6
PR4	< 2	27.8	6.1	192	< 5	29.5	< 3	2.1	7.09	44.26	32.33	5.68	0.078	0.47	0.23	1.19	6.71	1.805	0.21	6.73	99.71	30	6
PR5	5	167	8.6	183	< 5	27.1	< 3	4.6	6.95	45.87	29.98	5.38	0.065	0.72	0.23	1.18	6.11	1.837	0.16	7.15	98.69	28	6
PR6	8	57.2	8.1	117	< 5	17.6	< 3	6.8	6.90	60.93	20.63	5.48	0.081	0.28	0.18	0.98	3.68	1.288	0.17	4.68	98.37	19	4
PR7	< 2	36.3	0.8	73	< 5	11.0	< 3	1.1	8.35	62.13	18.17	8.76	0.045	0.20	0.10	0.61	2.97	0.854	0.10	5.24	99.18	12	3
PR8	< 2	39.2	14.6	110	< 5	16.4	< 3	7.3	6.53	63.96	17.59	6.48	0.071	0.30	0.04	0.92	3.38	0.921	0.05	4.97	98.68	17	4
PR9	< 2	19.3	4.2	123	< 5	17.4	< 3	4.2	6.51	63.33	19.97	4.86	0.025	0.30	0.04	0.77	3.89	0.989	0.05	4.81	99.03	18	4
PR10	< 2	37.4	7.6	128	< 5	18.4	< 3	4.6	6.25	54.38	20.84	10.58	0.043	0.39	0.05	0.75	3.68	0.941	0.05	6.47	98.17	19	4
PR11	< 2	21.0	6.7	129	< 5	16.9	< 3	2.3	6.24	61.67	19.58	7.60	0.087	0.30	0.08	0.80	3.57	1.193	0.16	5.28	100.3	18	4
PR12	< 2	21.1	< 0.5	130	< 5	17.7	< 3	2.1	6.41	58.69	21.35	6.67	0.129	0.27	0.09	0.78	3.92	1.256	0.10	5.31	98.56	19	4
PR13	< 2	43.9	6.7	127	< 5	17.4	< 3	2.8	6.94	54.15	20.78	10.37	0.473	0.37	0.06	0.81	3.89	1.248	0.12	6.29	98.57	19	4
PR14	< 2	86.0	7.1	101	< 5	13.7	< 3	4.4	6.43	67.55	16.08	5.12	0.050	0.23	0.04	0.72	3.18	0.909	0.07	3.99	97.93	14	3
PR15	5	132	< 0.5	103	< 5	16.7	< 3	6.1	7.13	63.34	19.04	7.11	0.177	0.31	0.05	0.71	4.09	1.118	0.08	4.44	100.5	17	3
PR16	5	430	2.7	127	< 5	20.9	< 3	12.2	6.82	54.66	24.03	5.95	0.121	0.37	0.05	0.98	5.02	1.309	0.08	5.43	98.00	21	5
PR17	< 2	17.3	4.3	121	< 5	17.2	< 3	4.8	6.61	62.45	21.07	3.84	< 0.005	0.22	0.03	0.81	4.02	1.024	0.05	4.32	97.85	18	3
PR18	< 2	11.1	4.6	119	< 5	17.9	< 3	2.0	6.19	60.06	21.75	6.27	0.049	0.30	0.05	0.78	4.00	0.953	0.05	5.23	99.50	19	4
PR19	< 2	27.9	6.8	120	< 5	17.2	< 3	3.4	6.06	64.62	22.87	1.79	< 0.005	0.26	0.04	0.93	4.07	1.101	0.05	4.51	100.3	19	3
PR20	< 2	10.9	1.2	116	< 5	15.3	< 3	1.9	8.62	67.46	22.39	0.49	< 0.005	0.22	0.03	0.87	4.23	1.067	0.04	3.76	100.5	16	4
PRC	< 2	24.1	14.9	123	< 5	19.4	< 3	3.1	8.08	61.42	22.27	4.43	0.042	0.38	0.04	1.11	3.91	1.174	0.05	5.78	100.6	20	4

Results **Activation Laboratories Ltd.** **Report: A23-04529**

Analyte Symbol	V	Cr	Co	Ni	Cu	Zn	Cd	S	Ga	Ge	As	Rb	Sr	Y	Zr	Nb	Mo	Ag	In	Sn	Sb	Cs	Ba
Unit Symbol	ppm	ppm	ppm	ppm	ppm	ppm	ppm	%	ppm	ppm	ppm	ppm	ppm	ppm	ppm	ppm	ppm	ppm	ppm	ppm	ppm	ppm	ppm
Lower Limit	5	20	1	1	1	1	0.5	0.001	1	0.5	5	1	2	1	1	0.2	2	0.3	0.1	1	0.2	0.1	2
Method Code	FUS-ICP	FUS-MS	FUS-MS	TD-ICP	TD-ICP	TD-ICP	TD-ICP	TD-ICP	FUS-MS	FUS-MS	FUS-MS	FUS-MS	FUS-ICP	FUS-ICP	FUS-ICP	FUS-MS	FUS-MS	TD-ICP	FUS-MS	FUS-MS	FUS-MS	FUS-MS	FUS-ICP
PR1	219	140	19	42	14	71	< 0.5	0.008	37	2.7	22	212	244	41	328	28.3	< 2	0.4	0.1	5	2.5	8.5	639
PR2	220	120	33	71	53	101	< 0.5	0.010	34	2.8	72	201	195	35	233	22.1	< 2	< 0.3	0.1	4	1.7	7.1	592
PR3	182	130	21	43	25	88	< 0.5	0.003	43	2.5	19	260	202	52	265	25.8	< 2	< 0.3	0.1	5	1.4	9.2	1086
PR4	211	170	19	45	15	83	< 0.5	0.005	46	2.7	22	289	256	63	458	34.0	< 2	0.5	0.1	6	2.0	9.6	1272
PR5	202	160	32	44	33	66	< 0.5	0.015	45	2.5	121	270	230	70	639	35.5	< 2	0.5	0.1	6	3.4	8.8	1155
PR6	134	100	27	53	22	83	< 0.5	0.010	31	2.4	55	163	289	46	366	21.0	6	0.3	0.1	4	6.0	5.9	655
PR7	97	70	25	43	19	111	< 0.5	0.005	25	2.5	30	133	118	32	273	13.2	< 2	< 0.3	< 0.1	3	0.7	4.6	525
PR8	154	100	13	46	26	90	< 0.5	0.017	31	2.5	39	164	149	31	226	14.7	< 2	< 0.3	0.1	6	6.0	5.9	634
PR9	161	110	12	38	21	69	< 0.5	0.005	29	2.5	15	191	154	28	219	15.7	< 2	< 0.3	0.1	3	3.2	7.3	589
PR10	171	110	26	86	31	177	< 0.5	0.012	30	3.1	34	176	144	23	149	14.0	< 2	< 0.3	0.1	3	3.9	6.9	544
PR11	133	120	23	69	22	93	< 0.5	0.009	28	2.4	17	166	197	40	320	20.6	< 2	0.3	0.1	4	1.6	5.6	647
PR12	139	120	26	54	30	95	< 0.5	0.003	31	2.6	19	178	204	40	375	21.2	< 2	0.4	0.1	4	1.4	6.3	735
PR13	139	120	69	88	34	132	< 0.5	0.007	31	2.6	44	179	234	44	447	22.6	< 2	< 0.3	0.1	4	2.5	6.5	1090
PR14	105	100	15	42	25	33	< 0.5	0.006	24	2.3	83	150	173	28	236	14.0	< 2	< 0.3	0.1	3	3.9	5.4	571
PR15	122	100	29	58	21	33	< 0.5	0.006	30	2.3	119	182	204	38	336	20.0	< 2	< 0.3	0.1	4	5.7	6.1	735
PR16	148	120	31	61	40	31	< 0.5	0.009	37	2.8	388	225	240	46	383	23.7	< 2	< 0.3	0.1	5	10.9	7.8	881
PR17	176	120	2	27	10	32	< 0.5	0.004	32	3.4	18	203	195	30	195	18.3	< 2	< 0.3	0.1	4	4.8	6.7	605
PR18	157	120	15	44	29	87	< 0.5	0.004	32	3.1	10	202	182	26	174	17.2	< 2	< 0.3	0.1	4	2.0	6.8	582
PR19	166	110	2	25	38	11	< 0.5	0.005	32	3.2	26	204	202	28	198	19.1	< 2	< 0.3	0.1	4	2.9	7.3	581
PR20	165	120	1	8	5	8	< 0.5	0.001	32	2.8	9	216	206	29	228	18.4	< 2	< 0.3	0.1	4	1.5	8.1	645
PRC	180	110	18	33	11	72	< 0.5	0.011	33	2.5	22	190	221	31	238	22.6	< 2	0.3	0.1	4	2.9	7.1	595

Results **Activation Laboratories Ltd.** **Report: A23-04529**

Analyte Symbol	La	Ce	Pr	Nd	Sm	Eu	Gd	Tb	Dy	Ho	Er	Tm	Yb	Lu	Hf	Ta	W	Tl	Pb	Bi	Th	U
Unit Symbol	ppm	ppm	ppm	ppm	ppm	ppm	ppm	ppm	ppm	ppm	ppm	ppm	ppm	ppm	ppm	ppm	ppm	ppm	ppm	ppm	ppm	ppm
Lower Limit	0.05	0.05	0.01	0.05	0.01	0.005	0.01	0.01	0.01	0.01	0.01	0.005	0.01	0.002	0.1	0.01	0.5	0.05	5	0.1	0.05	0.01
Method Code	FUS-MS	FUS-MS	FUS-MS	FUS-MS	FUS-MS	FUS-MS	FUS-MS	FUS-MS	FUS-MS	FUS-MS	FUS-MS	FUS-MS	FUS-MS	FUS-MS	FUS-MS	FUS-MS	FUS-MS	FUS-MS	TD-ICP	FUS-MS	FUS-MS	FUS-MS
PR1	72.4	145	16.6	59.2	11.4	1.99	8.26	1.25	7.94	1.56	4.79	0.680	4.56	0.750	9.3	2.14	3.4	0.85	< 5	0.2	22.3	4.47
PR2	57.3	108	13.1	48.2	9.03	1.73	6.94	1.04	6.67	1.31	4.03	0.550	3.86	0.647	6.3	1.79	3.4	0.80	< 5	0.1	18.0	3.64
PR3	80.8	162	19.0	71.3	14.4	2.75	11.9	1.72	10.5	1.97	5.75	0.788	5.37	0.823	7.5	1.94	3.0	1.08	< 5	0.1	22.0	4.38
PR4	99.5	201	23.1	86.2	17.3	3.26	13.6	2.02	12.3	2.32	7.04	0.987	6.84	1.04	12.6	2.58	4.7	1.21	< 5	< 0.1	28.1	6.20
PR5	104	209	24.2	88.4	17.6	3.34	13.9	2.08	13.1	2.63	7.78	1.13	7.69	1.19	17.9	2.70	4.0	1.09	< 5	0.3	29.5	6.61
PR6	71.4	144	16.5	59.7	11.6	2.14	9.39	1.34	8.57	1.70	4.99	0.698	4.74	0.734	9.6	1.73	3.0	0.69	13	0.5	19.9	4.30
PR7	55.3	112	13.0	50.0	10.2	1.86	8.13	1.14	6.60	1.23	3.62	0.489	3.16	0.500	7.1	1.09	1.9	0.57	< 5	< 0.1	14.2	2.91
PR8	48.2	93.6	10.9	41.5	9.07	1.09	6.79	0.98	5.96	1.12	3.44	0.482	3.15	0.512	5.7	1.31	2.7	0.90	12	0.3	14.7	3.87
PR9	48.3	97.3	11.0	41.0	7.44	1.30	5.80	0.90	5.46	1.07	3.19	0.464	2.99	0.510	5.6	1.28	2.5	0.74	< 5	0.2	15.0	2.97
PR10	46.4	91.1	10.5	38.0	6.68	1.38	5.35	0.79	4.85	0.92	2.85	0.403	2.73	0.418	3.9	1.20	1.6	0.72	7	0.3	14.0	2.62
PR11	62.1	122	14.6	54.7	10.8	1.98	9.21	1.34	7.97	1.55	4.52	0.620	4.02	0.672	8.5	1.70	2.2	0.66	< 5	0.2	17.8	3.83
PR12	69.0	141	16.1	59.9	11.8	2.00	8.85	1.28	7.75	1.52	4.71	0.654	4.40	0.736	10.2	1.72	2.8	0.81	< 5	0.2	19.9	4.16
PR13	72.3	159	16.6	60.3	12.4	2.24	10.0	1.43	8.73	1.66	5.10	0.697	4.73	0.766	11.9	1.76	2.5	0.88	< 5	0.3	21.0	4.45
PR14	47.7	93.9	11.4	43.2	8.33	1.53	6.40	0.93	5.60	1.11	3.32	0.473	3.27	0.512	6.5	1.34	1.7	0.67	< 5	0.4	14.1	3.08
PR15	60.5	117	13.8	50.3	10.5	1.99	8.72	1.25	7.70	1.49	4.52	0.609	4.31	0.683	9.2	1.56	2.7	0.81	7	0.3	17.8	3.43
PR16	74.8	150	17.3	63.6	13.3	2.56	10.8	1.55	9.42	1.81	5.23	0.734	5.09	0.827	10.7	1.87	3.2	1.02	14	1.1	22.1	4.08
PR17	43.3	85.2	9.85	37.1	7.40	1.36	6.11	0.98	6.30	1.23	3.53	0.512	3.35	0.520	5.6	1.46	2.6	0.85	5	0.2	15.1	2.54
PR18	43.6	85.6	9.31	34.9	6.74	1.32	5.30	0.86	5.17	1.01	3.12	0.441	2.94	0.469	5.0	1.33	2.0	0.83	< 5	0.2	15.1	2.47
PR19	53.9	107	11.8	43.5	7.82	1.43	5.97	0.90	5.62	1.09	3.29	0.448	3.19	0.500	5.4	1.49	2.3	0.82	9	0.3	16.7	2.65
PR20	52.2	112	12.0	43.9	8.21	1.33	6.17	0.90	5.73	1.15	3.52	0.493	3.39	0.550	6.4	1.41	2.6	0.93	< 5	< 0.1	16.8	2.91
PRC	50.7	102	11.9	44.3	8.30	1.43	6.46	0.94	6.12	1.21	3.76	0.530	3.70	0.606	6.7	1.69	3.2	0.68	< 5	0.1	16.6	3.45

Analyte Symbol	Au	As	Br	Cr	Ir	Sc	Se	Sb	Mass	SiO2	Al2O3	Fe2O3(T)	MnO	MgO	CaO	Na2O	K2O	TiO2	P2O5	Total	Sc	Be	V
Unit Symbol	ppb	ppm	ppm	ppm	ppb	ppm	ppm	ppm	g	%	%	%	%	%	%	%	%	%	%	%	ppm	ppm	ppm
Lower Limit	2	0.5	0.5	5	5	0.1	3	0.2		0.01	0.01	0.01	0.005	0.01	0.01	0.01	0.01	0.001	0.01	0.01	1	1	5
Method Code	INAA	INAA	INAA	INAA	INAA	INAA	INAA	INAA	INAA	FUS-ICP	FUS-ICP	FUS-ICP	FUS-ICP	FUS-ICP	FUS-ICP	FUS-ICP	FUS-ICP	FUS-ICP	FUS-ICP	FUS-ICP	FUS-ICP	FUS-ICP	FUS-ICP
NIST 694 Meas										10.47	1.82	0.78	0.012	0.34	42.93	0.86	0.53	0.111	30.40				1690
NIST 694 Cert										11.2	1.80	0.790	0.0116	0.330	43.6	0.860	0.510	0.110	30.2				1740
GBW 07113 Meas										69.25	12.73	3.22	0.137	0.15	0.59	2.46	5.34	0.287	0.05		5	4	< 5
GBW 07113 Cert										72.8	13.0	3.21	0.140	0.160	0.590	2.57	5.43	0.300	0.0500		5.00	4.00	5.00
SY-4 Meas										50.00	20.11	6.05	0.103	0.52	7.89	6.95	1.66	0.291	0.13		< 1	3	6
SY-4 Cert										49.9	20.69	6.21	0.108	0.54	8.05	7.10	1.66	0.287	0.131		1.1	2.6	8.0
BIR-1a Meas										48.26	15.51	11.05	0.166	9.68	13.39	1.83	0.03	0.983	0.02		43	< 1	325
BIR-1a Cert										47.96	15.50	11.30	0.175	9.700	13.30	1.82	0.030	0.96	0.021		44	0.58	310
ZW-C Meas																							
ZW-C Cert																							
OREAS 101b (Fusion) Meas																							
OREAS 101b (Fusion) Cert																							
OREAS 101b (4 Acid) Meas																							
OREAS 101b (4 Acid) Cert																							
OREAS 98 (4 Acid) Meas																							
OREAS 98 (4 Acid) Cert																							
NCS DC86318 Meas																							
NCS DC86318 Cert																							
USZ 25-2006 Meas																							
USZ 25-2006 Cert																							
DNC-1a Meas										46.93	18.24	9.61	0.143	10.05	11.25	1.91	0.22	0.474	0.07		31		149
DNC-1a Cert										47.15	18.34	9.97	0.150	10.13	11.49	1.890	0.234	0.480	0.07		31		148
OREAS 13b (4-Acid) Meas																							
OREAS 13b (4-Acid) Cert																							
BCR-2 Meas										54.70	13.59	13.67	0.190	3.57	7.26	3.06	1.79	2.272	0.37		33		433
BCR-2 Cert										54.1	13.5	13.8	0.196	3.59	7.12	3.16	1.79	2.26	0.35		33		416
USZ 42-2006 Meas																							
USZ 42-2006 Cert																							
OREAS 903 (4 Acid) Meas																							
OREAS 903 (4 Acid) Cert																							
OREAS 45d (4-Acid) Meas																							
OREAS 45d (4-Acid) Cert																							
REE-1 Meas																							
REE-1 Cert																							
OREAS 905 (INAA) Meas	377	37.5						2.4															
OREAS 905 (INAA) Cert	391	36.2						1.96															

Analyte Symbol	Au	As	Br	Cr	Ir	Sc	Se	Sb	Mass	SiO2	Al2O3	Fe2O3(T)	MnO	MgO	CaO	Na2O	K2O	TiO2	P2O5	Total	Sc	Be	V
Unit Symbol	ppb	ppm	ppm	ppm	ppb	ppm	ppm	ppm	g	%	%	%	%	%	%	%	%	%	%	%	ppm	ppm	ppm
Lower Limit	2	0.5	0.5	5	5	0.1	3	0.2		0.01	0.01	0.01	0.005	0.01	0.01	0.01	0.01	0.001	0.01	0.01	1	1	5
Method Code	INAA	INAA	INAA	INAA	INAA	INAA	INAA	INAA	INAA	FUS-ICP	FUS-ICP	FUS-ICP	FUS-ICP	FUS-ICP	FUS-ICP	FUS-ICP	FUS-ICP	FUS-ICP	FUS-ICP	FUS-ICP	FUS-ICP	FUS-ICP	FUS-ICP
OREAS 96 (4 Acid) Meas																							
OREAS 96 (4 Acid) Cert																							
Oreas 72b (4 Acid) Meas																							
Oreas 72b (4 Acid) Cert																							
W-2b Meas										53.12	15.65	10.79	0.160	6.33	10.90	2.21	0.62	1.089	0.15		36	< 1	271
W-2b Cert										52.4	15.4	10.7	0.163	6.37	10.9	2.14	0.626	1.06	0.140		36.0	1.30	262
OREAS 681 (4 Acid) Meas																							
OREAS 681 (4 Acid) Cert																							
Oreas 521 (4 Acid) Meas																							
Oreas 521 (4 Acid) Cert																							
OREAS 70b (4 Acid) Meas																							
OREAS 70b (4 Acid) Cert																							
OREAS 620 (4 Acid) Meas																							
OREAS 620 (4 Acid) Cert																							
PR1 Orig																							
PR1 Dup																							
PR15 Orig										63.31	19.07	7.14	0.177	0.31	0.05	0.71	4.09	1.108	0.09	100.5	17	3	122
PR15 Dup										63.37	19.01	7.09	0.178	0.32	0.05	0.71	4.09	1.127	0.08	100.5	18	3	122
PR18 Orig																							
PR18 Dup																							
PR19 Orig																							
PR19 Dup																							
Method Blank	< 2	< 0.5	< 0.5	< 5	< 5	< 0.1	< 3	< 0.2	10.0														
Method Blank										< 0.01	< 0.01	< 0.01	< 0.005	< 0.01	0.01	< 0.01	< 0.01	< 0.001	< 0.01		< 1	< 1	< 5
Method Blank																							
Method Blank																							
Method Blank																							

Analyte Symbol	Cr	Co	Ni	Cu	Zn	Cd	S	Ga	Ge	As	Rb	Sr	Y	Zr	Nb	Mo	Ag	In	Sn	Sb	Cs	Ba	La
Unit Symbol	ppm	ppm	ppm	ppm	ppm	ppm	%	ppm	ppm	ppm	ppm	ppm	ppm	ppm	ppm	ppm	ppm	ppm	ppm	ppm	ppm	ppm	ppm
Lower Limit	20	1	1	1	1	0.5	0.001	1	0.5	5	1	2	1	1	0.2	2	0.3	0.1	1	0.2	0.1	2	0.05
Method Code	FUS-MS	FUS-MS	TD-ICP	TD-ICP	TD-ICP	TD-ICP	TD-ICP	FUS-MS	FUS-MS	FUS-MS	FUS-MS	FUS-ICP	FUS-ICP	FUS-ICP	FUS-MS	FUS-MS	TD-ICP	FUS-MS	FUS-MS	FUS-MS	FUS-MS	FUS-ICP	FUS-MS
NIST 694 Meas																							
NIST 694 Cert																							
GBW 07113 Meas												42	46	392								504	
GBW 07113 Cert												43.0	43.0	403								506	
SY-4 Meas												1191	123	523								346	
SY-4 Cert												1191	119	517								340	
BIR-1a Meas		54										109	16	16								7	0.70
BIR-1a Cert		52										110	16	18								6	0.63
ZW-C Meas	60							107			> 1000				216				> 1000	4.5	262		30.2
ZW-C Cert	56.0							99			8500				198				1300	4.2	260		30.0
OREAS 101b (Fusion) Meas		45														19							777
OREAS 101b (Fusion) Cert		47														21							789
OREAS 101b (4 Acid) Meas			10	418																			
OREAS 101b (4 Acid) Cert			8.2	412																			
OREAS 98 (4 Acid) Meas				> 10000	1330		16.8										41.6						
OREAS 98 (4 Acid) Cert				14800 0.0	1360		15.5										45.1						
NCS DC86318 Meas											373										11.1		1940
NCS DC86318 Cert											369.42										11.88		1960
USZ 25-2006 Meas		35																					> 2000
USZ 25-2006 Cert		32.5																					19300
DNC-1a Meas												144	17	40								109	
DNC-1a Cert												144	18.0	38.0								118	
OREAS 13b (4-Acid) Meas			2120	2460	136		1.22										1.0						
OREAS 13b (4-Acid) Cert			2247.0 000	2327.0 000	133		1.2										0.86						
BCR-2 Meas												340	36	189								710	
BCR-2 Cert												346	37	188								683	
USZ 42-2006 Meas										241					34.0	35							> 2000
USZ 42-2006 Cert										224					31.00	34.40							21100
OREAS 903 (4 Acid) Meas			58	6750	29	< 0.5	0.491										0.4						
OREAS 903 (4 Acid) Cert			54.0	6520	24.3	0.200	0.500										0.432						
OREAS 45d (4-Acid) Meas			239	390	47		0.041																
OREAS 45d (4-Acid) Cert			231.0	371	45.7		0.049																
REE-1 Meas	290									122	> 1000				> 1000				488		1.1		1680
REE-1 Cert	277									124	1050				4050				498		1.07		1661
OREAS 905 (INAA) Meas																							
OREAS 905 (INAA) Cert																							
OREAS 96 (4				> 10000	455		4.39										11.1						

Analyte Symbol	Cr	Co	Ni	Cu	Zn	Cd	S	Ga	Ge	As	Rb	Sr	Y	Zr	Nb	Mo	Ag	In	Sn	Sb	Cs	Ba	La
Unit Symbol	ppm	ppm	ppm	ppm	ppm	ppm	%	ppm	ppm	ppm	ppm	ppm	ppm	ppm	ppm	ppm	ppm	ppm	ppm	ppm	ppm	ppm	ppm
Lower Limit	20	1	1	1	1	0.5	0.001	1	0.5	5	1	2	1	1	0.2	2	0.3	0.1	1	0.2	0.1	2	0.05
Method Code	FUS-MS	FUS-MS	TD-ICP	TD-ICP	TD-ICP	TD-ICP	TD-ICP	FUS-MS	FUS-MS	FUS-MS	FUS-MS	FUS-ICP	FUS-ICP	FUS-ICP	FUS-MS	FUS-MS	TD-ICP	FUS-MS	FUS-MS	FUS-MS	FUS-MS	FUS-ICP	FUS-MS
Acid) Meas																							
OREAS 96 (4 Acid) Cert				39300	457		4.19										11.5						
Oreas 72b (4 Acid) Meas			6420	224	95	< 0.5	1.47										0.4						
Oreas 72b (4 Acid) Cert			6860	222	99.0	0.310	1.49										0.230						
W-2b Meas	90	44								< 5	20	197	21	96	7.3					0.8		181	11.0
W-2b Cert	92.0	43.0								1.20	21.0	190	24.0	94.0	7.90					0.790		182	10.0
OREAS 681 (4 Acid) Meas			454	269	80		0.103										< 0.3						
OREAS 681 (4 Acid) Cert			503	264	88.0		0.109										0.118						
Oreas 521 (4 Acid) Meas			73	5930	25		1.77										1.1						
Oreas 521 (4 Acid) Cert			73	6070	24		1.80										0.89						
OREAS 70b (4 Acid) Meas			1950	54	101	< 0.5	0.292										< 0.3						
OREAS 70b (4 Acid) Cert			2180	52	112	0.4	0.309										0.2						
OREAS 620 (4 Acid) Meas			16	1810	> 10000	164	2.60										39.8						
OREAS 620 (4 Acid) Cert			15	1730	31500	163	2.47										38.5						
PR1 Orig			42	13	72	< 0.5	0.010										0.3						
PR1 Dup			42	14	70	< 0.5	0.007										0.4						
PR15 Orig	100	29						29	2.2	110	180	205	38	341	19.9	< 2		0.1	4	5.4	6.0	734	59.4
PR15 Dup	110	29						30	2.4	127	184	204	38	331	20.0	< 2		0.1	4	6.0	6.2	736	61.7
PR18 Orig			44	28	86	< 0.5	0.004										< 0.3						
PR18 Dup			44	29	87	< 0.5	0.003										< 0.3						
PR19 Orig			25	38	10	< 0.5	0.006										0.3						
PR19 Dup			25	38	11	< 0.5	0.004										< 0.3						
Method Blank																							
Method Blank												< 2	< 1	3								< 2	
Method Blank	< 20	< 1						< 1	< 0.5	< 5	< 1				< 0.2	< 2		< 0.1	< 1	< 0.2	< 0.1		< 0.05
Method Blank			< 1	< 1	< 1	< 0.5	< 0.001										< 0.3						
Method Blank			< 1	< 1	< 1	< 0.5	< 0.001										< 0.3						

Analyte Symbol	Ce	Pr	Nd	Sm	Eu	Gd	Tb	Dy	Ho	Er	Tm	Yb	Lu	Hf	Ta	W	Tl	Pb	Bi	Th	U
Unit Symbol	ppm	ppm	ppm	ppm	ppm	ppm	ppm	ppm	ppm	ppm	ppm	ppm	ppm	ppm	ppm	ppm	ppm	ppm	ppm	ppm	ppm
Lower Limit	0.05	0.01	0.05	0.01	0.005	0.01	0.01	0.01	0.01	0.01	0.005	0.01	0.002	0.1	0.01	0.5	0.05	5	0.1	0.05	0.01
Method Code	FUS-MS	FUS-MS	FUS-MS	FUS-MS	FUS-MS	FUS-MS	FUS-MS	FUS-MS	FUS-MS	FUS-MS	FUS-MS	FUS-MS	FUS-MS	FUS-MS	FUS-MS	FUS-MS	FUS-MS	TD-ICP	FUS-MS	FUS-MS	FUS-MS
NIST 694 Meas																					
NIST 694 Cert																					
GBW 07113 Meas																					
GBW 07113 Cert																					
SY-4 Meas																					
SY-4 Cert																					
BIR-1a Meas	2.00		2.40	1.10	0.510							1.60	0.270	0.6							
BIR-1a Cert	1.9		2.5	1.1	0.55							1.7	0.3	0.60							
ZW-C Meas	101	9.70	25.9	7.00		4.50			1.90		1.60	14.8	2.32	9.8	82.0	291	33.0			45.0	19.4
ZW-C Cert	97	9.5	25.0	6.6		4.70			2.0		1.60	14	2.20	9.7	82	320	34			43	20.0
OREAS 101b (Fusion) Meas	1330	125	388	49.0	7.76		5.28	31.4	6.27	18.7	2.68	17.7	2.66							37.3	404
OREAS 101b (Fusion) Cert	1331	127	378	48	7.77		5.37	32.1	6.34	18.7	2.66	17.6	2.58							37.1	396
OREAS 101b (4 Acid) Meas																		21			
OREAS 101b (4 Acid) Cert																		23			
OREAS 98 (4 Acid) Meas																		279			
OREAS 98 (4 Acid) Cert																		345			
NCS DC86318 Meas	408	719	> 2000	> 1000	18.6	> 1000	467	> 1000	576	> 1000	265	> 1000	253							67.6	
NCS DC86318 Cert	432	737	3429	1725	18.91	2168	468	3224	560	1750	271	1844	264							67.0	
USZ 25-2006 Meas	> 3000	> 1000		835	195							49.9									
USZ 25-2006 Cert	29000	2800		900	211.00							54.5									
DNC-1a Meas																					
DNC-1a Cert																					
OREAS 13b (4-Acid) Meas																					
OREAS 13b (4-Acid) Cert																					
BCR-2 Meas																					
BCR-2 Cert																					
USZ 42-2006 Meas	> 3000	> 1000	> 2000	513	86.0				7.59			17.0								929	
USZ 42-2006 Cert	27600	2300	6500	539	87.22				7.86			17.85								946	
OREAS 903 (4 Acid) Meas																		11			
OREAS 903 (4 Acid) Cert																		11.3			
OREAS 45d (4-Acid) Meas																		19			
OREAS 45d (4-Acid) Cert																		21.8			
REE-1 Meas	> 3000	450	1480	402	24.3	432	111	889	208	722	109	702		486						765	142
REE-1 Cert	3960	435	1456	381	23.5	433	106	847	208	701	106	678		479						719	137
OREAS 905 (INAA) Meas																					
OREAS 905 (INAA) Cert																					
OREAS 96 (4																		85			

Analyte Symbol	Ce	Pr	Nd	Sm	Eu	Gd	Tb	Dy	Ho	Er	Tm	Yb	Lu	Hf	Ta	W	Tl	Pb	Bi	Th	U
Unit Symbol	ppm	ppm	ppm	ppm	ppm	ppm	ppm	ppm	ppm	ppm	ppm	ppm	ppm	ppm	ppm	ppm	ppm	ppm	ppm	ppm	ppm
Lower Limit	0.05	0.01	0.05	0.01	0.005	0.01	0.01	0.01	0.01	0.01	0.005	0.01	0.002	0.1	0.01	0.5	0.05	5	0.1	0.05	0.01
Method Code	FUS-MS	FUS-MS	FUS-MS	FUS-MS	FUS-MS	FUS-MS	FUS-MS	FUS-MS	FUS-MS	FUS-MS	FUS-MS	FUS-MS	FUS-MS	FUS-MS	FUS-MS	FUS-MS	FUS-MS	TD-ICP	FUS-MS	FUS-MS	FUS-MS
Acid) Meas																					
OREAS 96 (4 Acid) Cert																		101			
Oreas 72b (4 Acid) Meas																		12			
Oreas 72b (4 Acid) Cert																		14.9			
W-2b Meas	23.9		13.3	3.50	1.00		0.59	3.80	0.75	2.30		2.00	0.320	2.5	0.50					2.20	0.58
W-2b Cert	23.0		13.0	3.30	1.00		0.630	3.60	0.760	2.50		2.10	0.330	2.60	0.500					2.40	0.530
OREAS 681 (4 Acid) Meas																		6			
OREAS 681 (4 Acid) Cert																		10.2			
Oreas 521 (4 Acid) Meas																		9			
Oreas 521 (4 Acid) Cert																		9			
OREAS 70b (4 Acid) Meas																		14			
OREAS 70b (4 Acid) Cert																		14			
OREAS 620 (4 Acid) Meas																		> 5000			
OREAS 620 (4 Acid) Cert																		7740			
PR1 Orig																		< 5			
PR1 Dup																		< 5			
PR15 Orig	115	13.6	49.6	10.3	1.98	8.64	1.25	7.61	1.48	4.54	0.606	4.29	0.684	9.1	1.57	2.9	0.78		0.3	17.5	3.34
PR15 Dup	118	14.0	51.1	10.6	2.01	8.80	1.26	7.78	1.50	4.50	0.613	4.32	0.682	9.3	1.54	2.5	0.85		0.3	18.1	3.52
PR18 Orig																		< 5			
PR18 Dup																		< 5			
PR19 Orig																		9			
PR19 Dup																		9			
Method Blank																					
Method Blank																					
Method Blank	< 0.05	< 0.01	< 0.05	< 0.01	< 0.005	< 0.01	< 0.01	< 0.01	< 0.01	< 0.01	< 0.005	< 0.01	< 0.002	< 0.1	< 0.01	< 0.5	< 0.05		< 0.1	< 0.05	< 0.01
Method Blank																		< 5			
Method Blank																		< 5			